DOKUZ EYLÜL UNIVERSITY
GRADUATE SCHOOL OF NATURAL AND APPLIED SCIENCES

PRODUCTION AND DEVELOPMENT OF BIO-BASED UV-CURABLE NANOCOMPOSITE RESINS

by
Dilek Burcu YILDIZ

February, 2024
İZMİR

PRODUCTION AND DEVELOPMENT OF BIO-BASED UV-CURABLE NANOCOMPOSITE RESINS USED IN 3D PRINTING

A Thesis Submitted to the
Graduate School of Natural and Applied Sciences of Dokuz Eylül University
In Partial Fulfillment of the Requirements for Master of Science in
Department of Nanoscience and Nanoengineering, Nanoscience and Nanoengineering Program

by

Dilek Burcu YILDIZ

February, 2024
İZMİR

THESIS EXAMINATION RESULT FORM

We have read the thesis entitled **"PRODUCTION AND DEVELOPMENT OF BIO-BASED UV-CURABLE NANOCOMPOSITE RESINS"** completed by **DİLEK BURCU YILDIZ** under supervision of **ASSOC.PROF.DR. SERDAR YILDIRIM** and we certify that in our opinion it is fully adequate, in scope and in quality, as a thesis for the degree of. Master of Science.

Assoc.Prof.Dr. Serdar YILDIRIM
Supervisor

Assoc. Prof. Dr. Mustafa EROL
Jury Member

Assist. Prof. Dr. Savaş ÖZTÜRK
Jury Member

Prof. Dr. Okan FISTIKOĞLU
Director
Graduate School of Natural and Applied Sciences

ACKNOWLEDGMENT

I would like to thank everyone who supported me throughout my process to obtain my master's degree.

First of all, I would like to thank Associate Professor Serdar YILDIRIM, who guided me with understanding throughout the thesis process and helped me complete this process with his contributions and encouragement.

I would like to express my most special thanks to Dokuz Eylül University, Center of Electronic Materials Production and Application (EMUM), its employees, researchers and the resources they provide. I would like to thank NanoRes Co. for material supply and analysis support.

I would like to thank Berk ÖZLER for giving all the support he could whenever I needed help. Also I give my thanks Neslihan ŞAKAR for her emotional support and encouragement.

Most importantly and lastly, the fact that my beloved family supported me throughout this process, as always, motivated me. I would like to thank my father Bedri YILDIZ, my mother Cihan YILDIZ and my brother Bedirhan YILDIZ for their love, support and always being by my side.

Dilek Burcu YILDIZ

PRODUCTION AND DEVELOPMENT OF BIO-BASED UV-CURABLE NANOCOMPOSITE RESINS

ABSTRACT

Biobased resins, derived mainly from soybean oil, represent an eco-friendly option in the realm of 3D printing. Despite their environmentally conscious nature, these resins are often overshadowed by their mechanically superior counterpart, epoxy resins. To address the inherent limitations of biobased resins, a potential solution lies in nanoparticle reinforcement. The addition of nanoparticles to the resin aims to enhance mechanical properties, yet challenges arise due to their tendency to aggregate, leading to suboptimal outcomes.

This thesis focuses on the incorporation of silica (SiO_2) nanoparticles into biobased resin, coupled with a silanization process to mitigate aggregation. The ensuing investigation delves into the transformation degrees and alterations in mechanical properties of the resultant samples. SiO_2 nanoparticles, synthesized through the sol-gel method, underwent a silanization process before being blended with biobased resin in varying compositions. Throughout the sample preparation stages, XRD, SEM, FT-IR, three-point bending, and tensile test characterizations were meticulously conducted.

The sample containing 1.5 percent silanated nanoparticles and sample containing 5 percent silanated nanoparticles samples exhibited notable increases in the conversion degree 8.5 percent and 9.1 percent, respectively. Among the bending strength values, the sample containing 1.5 percent silanated nanoparticles demonstrated the highest at 91.68 MPa, while the SEC0.5 sample led in elastic modulus values with 3.01 GPa. The comprehensive characterizations unveiled the positive impact of both nanoparticle additives and silanization on mechanical properties and transformation degrees. Consequently, this study elucidates those biobased resins, when fortified with silanized SiO_2 nanoparticle additives, can be harnessed without compromising on performance.

Keywords: Photopolymer, nanocomposite, biobased, additive manufacturing.

BİYO BAZLI UV İLE KÜRLENEBİLİR NANOKOMPOZİT REÇİNE ÜRETİMİ VE GELİŞTİRİLMESİ

ÖZ

Üç boyutlu yazıcılarda kullanılan birçok farklı reçine türünden biri de çevre dostu olmasıyla bilinen ve genelde soya fasulyesi yağından elde edilen biyobazlı reçinelerdir. Kullanımı yaygın olan epoksi reçinelere kıyasla daha düşük mekanik özellik gösteren biyobazlı reçineler, bu sebeple fazla tercih edilmezler. Bu dezavantajı elimine etmek için başvurulacak yöntemlerden biri ise nanopartikül takviyesidir. Reçine içine ilave edilen bu nanopartiküller, topaklanma eğilimi gösterdiklerinden, mekanik özellikler ve dönüşüm dereceleri gibi değerlerde istenilen sonuç alınamayabilir. Bu tez kapsamında, silika (SiO_2) nanopartikülleri biyobazlı reçine içine ilave edilmiş ve topaklanmanın önüne geçmek için silanizasyon işlemine tabi tutulmuş ve hazırlanan numunelerin dönüşüm dereceleri, mekanik özelliklerindeki değişim incelenmiştir. SiO_2 nanopartikülleri sol-jel yöntemi kullanılarak sentezlenmiş ve ardından silanizasyon işlemine tabi tutulmuştur. Daha sonra farklı kompozisyonlarda biyobazlı reçine ile karıştırılarak standartlara uygun eğme ve çekme numuneleri oluşturulmuştur. Numuneler hazırlanırken her bir üretim aşamasının ardından XRD, SEM, FT-IR, üç noktalı eğme ve çekme testi karakterizasyonları yapılmıştır. Dönüşüm derecesinde yüzde 1.5 nanopartikül içeren numune ile yüzde 5 katkılı numuneler sırasıyla yüzde 8.5 ve yüzde 9.1'lik artış göstermiştir. Eğme mukavemeti değerlerinde 91.68 MPa ile en yüksek değeri SEC1.5 numunesi, elastisite modülü değerlerinde 3.01 GPa ile en yüksek değeri SEC0.5 numunesi vermiştir. Yapılan karakterizasyonlar sonucunda hem nanopartikül katkısının hem de nanopartiküllerin silanizasyon işlemine tabi tutulmasının mekanik özellikler ve dönüşüm derecelerine pozitif yönde etki yaptığı görülmüştür. Bu anlamda, biyobazlı reçinelerin, silanize edilmiş SiO_2 nanopartikül katkılarıyla desteklendiğinde, dezavantaja mahal vermeden kullanılabileceği anlaşılmıştır.

Anahtar kelimeler: Fotopolimer, nanokompozit, biyobazlı, eklemeli imalat.

CONTENTS

Page

THESIS EXAMINATION RESULT FORM ii
ACKNOWLEDGMENT iii
ABSTRACT iv
ÖZ v
LIST OF FIGURES viii
LIST OF TABLES x

CHAPTER ONE - INTRODUCTION 1
1.1 Background 1
1.2 Organization of the Thesis 4

CHAPTER TWO - THEORETICAL BACKGROUND 5
2.1 3D Printers Types and Additive Manifacturing 5
2.1.1. Fused Deposition Modelling 6
2.1.2. Direct Metal Laser Sintering (DMLS) 7
2.1.3. Selective Laser Sintering (SLS) 8
2.1.4. Binder Jetting Method 9
2.1.5. Material Jetting Method 11
2.1.6. Stereolithography (SLA) and Digital Light Processing (DLP) Method 11
2.2 Photosensitive Resin 12
2.2.1. Monomers and Oligomers 14
2.2.2. Photoinitiators 14
2.2.2.1. Conversion Degree 16
2.2.3. Fillers 16
2.3 Nanoparticles 17
2.3.1. Production Methods 17
2.3.1.1. Sol-Gel Method 18
2.3.2. Silanization 20

CHAPTER THREE - LITERATURE REVIEW 22
3.1 Biobased Nanocomposite Resins for 3D Printing 22

CHAPTER FOUR - EXPERIMENTAL STUDIES 26
4.1 Purpose 26
4.2 Materials 26
4.3 Methods 26
4.4 Characterization 30
4.4.1 Scanning Electron Microscopy (SEM) 30
4.4.2 X-Ray Diffraction (XRD) 31
4.4.3 Fourier Transform Infrared Spectroscopy (FT-IR) 32
4.4.4 X-Ray Photoelectron Spectroscopy (XPS) 33
4.4.5 Particle Size Distribution (PSD) 35
4.4.6 Thermogravimetric and Differential Thermal Analysis (TG/DTA) 35
4.4.7 Viscosimetry 36
4.4.8 Mechanical Tests 36
4.4.8.1 Three Point Bending Test 36
4.4.8.2 Tensile Test 37

CHAPTER FIVE - RESULTS AND DISCUSSION 40
5.1 Characterization of Nanoparticles 40
5.1.1 Structural Properties 40
5.1.2 Thermal Properties 40
5.1.3 Morphological Properties 41
5.1.4 Organic Bond Structures 42
5.1.5 Particle Size 43
5.2 Characterization of Nanocomposite Resins 44
5.2.1 Morphological Properties 44
5.2.2 Organic Bond Structures 47
5.2.3 Mechanical Properties 48
CHAPTER SIX - CONCLUSION AND FUTURE WORKS 58
REFERENCES 59

LIST OF FIGURES

Page

Figure 2.1 FDM Printer Scheme 7
Figure 2.2 Scheme of DMLS 8
Figure 2.3 SLS Scheme 9
Figure 2.4 Binder Jetting Method Scheme 10
Figure 2.5 Scheme of Material Jetting Method 11
Figure 2.6 SLA and DLP type 3D Printers Schemes 12
Figure 2. 7 Sythesis of Nanoparticles Scheme 18
Figure 2.8 Flowchart of Sol-Gel Method 19
Figure 2.9 Impression of Silanization 20
Figure 3.1 Production of ESO 22
Figure 3.2 Synthesis of AESO 23
Figure 3.3 TEGDMA Chain Structure 23
Figure 4.1 Process Scheme of Synthesis and Analysis 27
Figure 5.1 XRD Spectra of SiO2 Nanoparticles 40
Figure 5.2 TG/DTA analysis of SiO2 Nanoparticles 41
Figure 5.3 SEM images of SiO2 nanoparticles with 50K and 100K magnitude... 42
Figure 5.4 FT-IR Spectra of unsilanized and silanized SiO2 nanoparticles 43
Figure 5.5 Particle Size Distribution of SiO2 Nanoparticles 44
Figure 5.6 SEM images of ecoresin (a) EC1.5 (b) SEC1.5 (c) 45
Figure 5.7 X-Ray of ecoresin (a) EC1.5 (b) SEC1.5 (c) 47
Figure 5.8 FT-IR chart of SEC 1.5 sample before and after curing 48
Figure 5.9 Conversion Degrees of Samples 49
Figure 5.10 Elasticity Modulus Graph of Samples 50
Figure 5.11 Flexural Strenghts of Samples 51
Figure 5.12 Yield Strengths of Samples 52
Figure 5.13 Hardness Values of Samples 53
Figure 5.14 XPS Spectra of SEC1.5 Sample 53
Figure 5.15 XPS Spectra of EC1.5 Sample 54
Figure 5.16 XPS Spectra of EC Sample 55
Figure 5.17 XRD Spectra of Composites 56

Figure 5.18 DTA-TGA graph of EC (a), SEC1,5 (b) and EC1,5 (c) 57
Figure 5.19 Rheometer measurement of nanocomposites..... 58

LIST OF TABLES

Page

Table 2.1 Common Photoinitiators 15
Table 3.1 Literature Review 24
Table 4.1 Contents and nomenclature of composite resins 28
Table 5.1 XPS Analysis Contents of SEC1.5 54
Table 5.2 XPS Analysis Contents of EC1.5 54
Table 5.3 XPS Analysis Contents of EC 55
Table 5.4 Viscosity Values 59

CHAPTER ONE
INTRODUCTION

1.1 Background

Three-dimensional printing technologies have become popular in both daily use and industrial production (for example, personalized consumer products, dentistry, food industry, pharmaceutical industry, biomaterials industry) in recent years, but it is a method with many advantages. In its simplest form, three-dimensional printers are devices that enable the data stored in the computer environment to be converted into physical real objects through computer aided design (CAD). This technology can also produce geometries that cannot be achieved with traditional manufacturing methods. This technology, called three-dimensional (3D) production, is a form of production that has taken place in the literature as desktop manufacturing or additive manufacturing. Many different technologies are used to carry out production with these printers. Among these technologies, the most used are the Combined Stacking Model- FDM (Fused Deposition Modeling), Selective Laser Sintering- SLS (Selective Laser Sintering), Scanning Light Curing Technique- SLA (Stereo Lithography Apparatus), Laminated Adhesive Part Manufacturing- LOM (Laminated Object Manufacturing) can be sorted. Among these methods, the Light Curing Technique (SLA), which works on the photochemical principle, is extremely attractive and useful for the creation and production of finely detailed objects by photopolymerization of liquid photo-crosslinkable resins under UV-light. It is also important in terms of environmental (eg low amount of volatile organic compounds), economic (low energy consumption) and production benefits (variation of spatial and temporal control). (Silva et al., 2021)

In three-dimensional printers working with the photochemical principle, light-polymerizable resins are used as building materials. These materials, also known as photopolymers, are polymers that chemically change under UV light and laser beams. The material to be produced on this basis; These resins, photocurable, are composed of monomers, oligomers, photoinitiators, and, optionally, additional nanoparticles and color pigments. Photocurable resins are light-sensitive polymer-based materials that change their properties when exposed to UV light. The monomer and oligomer

compositions in the photocurable resins determine the mechanical properties (strength, hardness, shrinkage rate, viscosity). To eliminate this effect, diluent monomers that provide flexibility can be added to monomers with high viscosity and thus strength values. These flexible diluent monomers are generally long-chain monomers with low viscosity, low glass transition temperature, and high shrinkage rates. When this monomer mixture is exposed to light of appropriate wavelength with the help of photoinitiators added to the reaction vessel, they form crosslinks and bond to each other and the targeted polymer is obtained. Photocurable resins are polymerized with a photoinitiator added to them. The photoinitiator absorbs the light of the appropriate wavelength, and the reagents formed as a result of this absorption allow the monomers in the structure of the resin to cross-link and combine and thus solidify. (Xu et al., 2021)

These monomers with diluent monomer and photoinitiator added are in great demand in the industry as epoxy resin. Epoxy resins, also called polyepoxides, are resistant to water, alkali and acid. They are used in many industrial applications for various purposes, for example; industrial coatings, fiber reinforced plastics, aerospace industry, automotive industry etc. They are highly preferred due to their high mechanical properties and thermal-chemical resistance. However, with the developing industry, they feed the increasing waste production and thus the recycling problem. Today, approximately 90% of epoxy thermosets are obtained from bisphenol-A diglycidyl ether type epoxy monomers obtained by the reaction of epichlorohydrin and bisphenol-A in the presence of sodium hydroxide. The fact that almost all of the epoxy production is dependent on fossil sources does not seem appropriate to limit greenhouse gas emissions, and as a result, they cause an increase in global warming effects. These epoxy resins, which can show biocompatible properties according to their areas of use, are not biobased, nor do they show biodegradable properties, and in this context, they cannot be included under the umbrella of "green engineering", which is on the rise all over the world. The shift towards environmental sustainability in the worldwide economy, heightened awareness of carbon footprint implications, a growing focus on sustainable practices, and the advancement of life cycle analysis for products have prompted numerous manufacturers of thermoset resins to transition from reliance on oil and gas sources to the production of resins derived from plants.

Resin production from corn and soybean oil has been on the rise as it is environmentally friendly. A bioresin is a resin that obtains some or all of its constituent monomers from biological sources. In this direction, research has been carried out to develop biobased epoxy thermosets from renewable resources such as vegetable oils, furan, tannin, lignin, rosin, vanillin, daidzein and itaconic acid in order to replace petroleum-based epoxy systems. The obtained bio-based epoxies come to the fore as they show comparable properties to their petroleum-based counterparts and are environmentally friendly. (Voet et al., 2021)

In studies where oils obtained from plants (triglyceride) are used as a renewable resource, polymers are obtained by chemically modifying triglycerides, especially ester groups, carbon-carbon double bonds and allylic carbon groups. The most used oils in the literature are; soybean, flax, tung tree, palm, sunflower, corn, canola, cotton and castor oil plants. Upon reviewing the existing literature, it becomes evident that biobased resins are commonly derived from soybean oil, specifically Epoxidized Soybean Oil (ESO). This category of biobased epoxy constitutes a material acquired through the epoxidation process of soybean oil using hydrogen peroxide (H2O2) and acetic acid (or formic acid). This conversion involves transforming double bonds into epoxy groups, which are both non-toxic and possess higher chemical reactivity. To optimize additive production, epoxidized soybean oil must undergo acrylation, resulting in the formation of Acrylate Epoxidized Soybean Oil (AESO). The synthesis of AESO involves the reaction between epoxidized soybean oil and acrylic acid. Notably, the mechanical properties of biobased curable resins are observed to be inferior to those of commercially available epoxy resins. (Altuna et al., 2011)

One of the frequently used ways to strengthen mechanical properties is the addition of nanoparticles. Silica (SiO_2) was chosen as the Fillers. Silica nanoparticles come to the forefront with their high UV absorbance (200-700 nm), positive contribution to the conversion rate, and positively increasing biocompatibleand mechanical properties. Since it is aimed that the material to be obtained is biobased, biodegradable, and exhibits high mechanical properties, it is important to select the additive to be added to the resin with precision. (Guleria et al., 2016)

As a disadvantage of using SiO_2, agglomeration tendency can be shown. After adding to the resin, agglomerated SiO_2 nanoparticles should be prevented from

agglomeration, as it will negatively affect the mechanical properties. To prevent this, the silanization method was used. Thus, agglomeration of nanoparticles and thus a decrease in mechanical properties is prevented. (Sprenger S., 2013)

1.2 Organization of the Thesis

Within the scope of this thesis, different compositions of SiO_2 nanoparticles were added to the bio-based resin and the printability of this mixture was tested with a three-dimensional printer. The aim of the thesis is to obtain a nanocomposite with increased mechanical properties by using SiO_2 nanoparticles of bio-based resins, which have low mechanical properties compared to commercial epoxy resins but are used to maintain ecological balance.

Chapter 1 involves the 3D printers and the use of biobased resin in these printers and the purpose of writing this thesis.

Chapter 2, contains theoretical information about 3D printers, photopolymers, nanoparticles and their production methods and nanocomposites.

In Chapter 3, the literature overview on biobased photopolymer resins is found.

In Chapter 4, production and characterization stages of SiO_2 nanoparticles, production, printing and characterization methods of nanocomposite resins are explained in detail. The chemicals used in the synthesis and surface modification of nanoparticles are also given in this section.

In Chapter 5, the characterization results of the produced samples are given, these results are examined and explained with their reasons.

Chapter 6 is the last chapter that includes the conclusion of this thesis and plans for the future.

CHAPTER TWO
THEORETICAL BACKGROUND

2.1 3D Printer Types and Additive Manufacturing

Layered manufacturing, also known as additive manufacturing, stands as a pragmatic production approach founded on the concept of overlaying layers crafted in alignment with the three-dimensional (3D) geometric specifications of objects. This method employs a spectrum of materials, including metal, plastic, composite, and organic substances. Historically recognized as rapid prototyping, additive manufacturing has been predominantly employed for the fabrication of prototypes (Jacobs, P. F., 1992).

3D printers are a technology that has only existed in our lives for the past four decades. Thanks to the developments in the field of engineering and technology, it has reached its current qualifications. (Kabir et al., 2020)

The 3D Systems firm first popularized this technique in the 1980s using stereolithography (Stereolithograph-SL) technology. During the initial years of the 1990s, SL was succeeded by the commercialization and promotion of technologies such as Laminated Object Manufacturing (LOM) by Helysis Company, Fused Deposition Modeling (FDM) by Stratasys Company, Selective Laser Sintering (SLS) by DTM Company, and Direct Metal Powder Laser Sintering (Direct Metal Laser Sintering-DMLS) by EOS Company. The terminology associated with these technologies, which are gaining widespread adoption for additive manufacturing and prototyping, has concurrently started being identified as "3D printing." (Sürmen, H. K., 2019)

Three-dimensional printers are an additive manufacturing method in which objects are produced in layers using CAD programs without the need for a mold. Since they do not produce in accordance with a certain mold, they ensure the production of original and wide variety of products. After the design of a three-dimensional model is completed, it is layered with computer-aided design (CAD). Next, the 3D printer builds these layers on top of each other, creating the targeted product. These printers, which were previously used to obtain a rapid prototype of the desired product, are now frequently used to produce the final product.

Categorization of 3D printers is based on their manufacturing techniques, encompassing fused deposition modeling (FDM), stereolithography (SLA), digital light processing (DLP), selective laser sintering (SLS), laser metal deposition (LMD), and direct metal laser sintering (DMLS). (Ho et al., 2015)

2.1.1. Fused Deposition Modelling

Fused Deposition Modeling (FDM) stands as a prevalent technique in 3D printing, constituting a form of additive manufacturing that constructs three-dimensional objects through layer-by-layer fabrication which can be seen in Figure 2.1. FDM, being among the pioneering 3D printing methodologies, maintains its widespread adoption in the field. The sequential stages of production encompass the initial phase of model design, where the process commences with the development of a 3D digital model utilizing computer-aided design (CAD) software. Subsequently, this model undergoes segmentation into slender horizontal layers through slicing software, which then generates directives for the 3D printer. The ensuing phase involves the utilization of a thermoplastic filament as the foundational material in FDM printers. These filaments, used in spools, are obtained from different colors and materials such as ABS (acrylonitrile butadiene styrene), PLA (polylactic acid) and PETG (polyethylene tetraphthalate glycol). The next step is heating and extrusion; the 3D printer's print head, also called the extruder, contains a small nozzle through which the thermoplastic filament is fed. The nozzle is heated to melt the filament, turning it into a semi-liquid state. After this step, the next one is layer-by-layer deposition; the 3D printer moves its print head along the X, Y, and Z axes, following the instructions from the slicing software. It deposits the melted filament in the desired pattern on the build platform, one layer at a time. The next step is solidification; once a layer of the object is deposited, the melted filament quickly cools and solidifies, adhering to the layer below it. After that, build platform lowering; after completing one layer, the build platform is lowered or moved down by a small distance (typically the height of one layer), and the process is repeated for the next layer. The last step is completion; the printer continues the layer-by-layer deposition and solidification process until the entire 3D object is created. In addition, Fused Deposition Modeling offers several advantages, including ease of use, material variety, affordability, support structures. However, it's

essential to note that FDM has some limitations as well; layer lines and lower resolution. When examining low resolution, FDM printers may not attain the identical degree of intricacy and accuracy as certain alternative 3D printing techniques, like stereolithography (SLA) or selective laser sintering (SLS). Notwithstanding its constraints, FDM persists as one of the extensively employed 3D printing methods owing to its adaptability, user-friendly nature, and cost-efficiency. These attributes render it a favored option for a diverse range of applications encompassing prototyping, manufacturing, education, and personal projects in the realm of hobbies. (Penumakala et al., 2020)

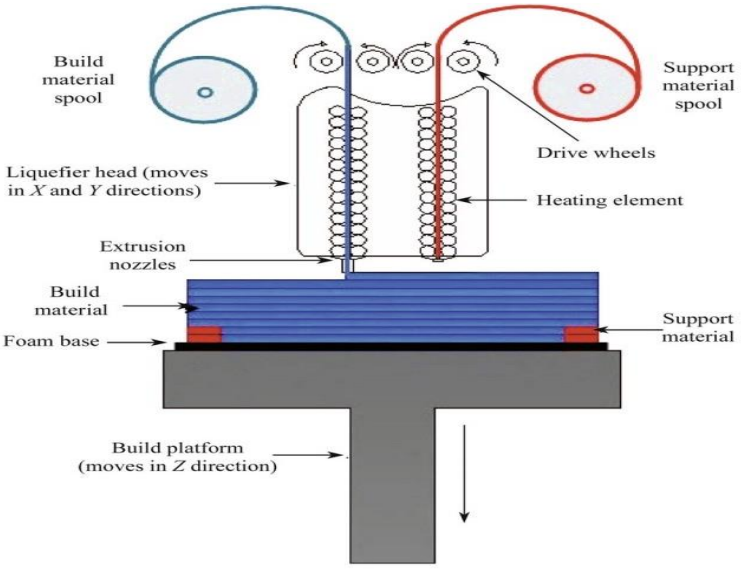


Figure 2.1 FDM Printer Scheme (Mohamed et al., 2015)

2.1.2. Direct Metal Laser Sintering (DMLS)

DMLS is a specific method used for creating three-dimensional objects by selectively fusing metal powder particles together using a high-powered laser. The process involves layer-by-layer construction, where each layer of the object is melted and solidified on top of the previous one until the entire object is formed. The working mechanism, which also can be seen in Figure 2.2, as follows; 3D model preparation, preparation of the build bed, laser sintering, layer-by-layer build, cooling and support removal and the last one is post-processing. DMLS is particularly suitable for producing intricate and complex metal parts with high accuracy, making it popular in various industries, including aerospace, automotive, medical, and engineering. It

facilitates the creation of operational prototypes and finished components, showcasing outstanding mechanical characteristics and surface textures. (Nandy et al., 2019)

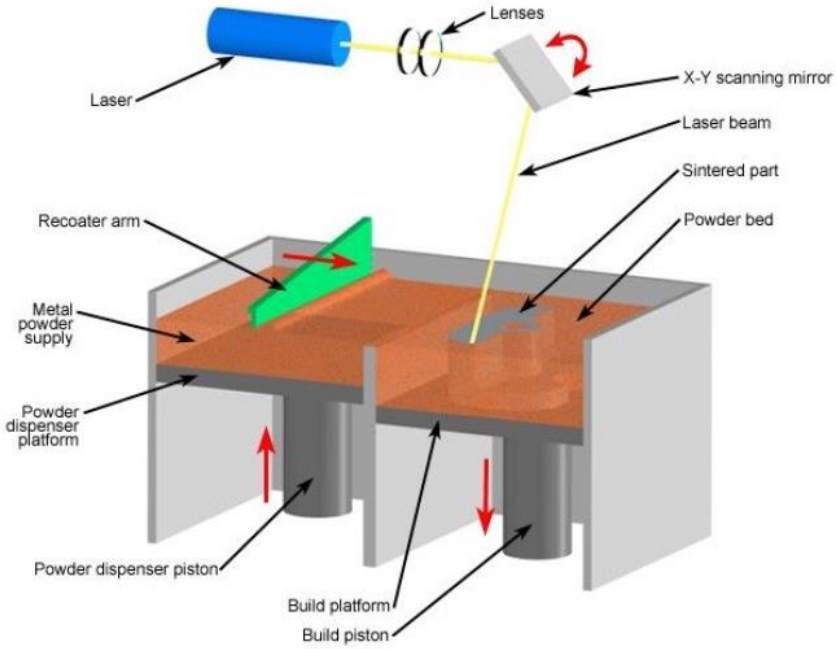


Figure 2.2 Scheme of DMLS (Verma et al., 2015)

2.1.3. Selective Laser Sintering (SLS)

Selective Laser Sintering (SLS) stands as an additive manufacturing (3D printing) technique utilizing a high-powered laser to selectively meld powdered materials, typically encompassing plastic, metal, or ceramic, resulting in the creation of three-dimensional objects. Widely acknowledged as one of the most employed and adaptable 3D printing technologies, SLS offers numerous advantages in comparison to alternative additive manufacturing methods. The initial phase within the SLS operational process involves material readiness, commencing with a bed hosting the chosen powdered material, commonly nylon (polyamide) for plastics or metals like aluminum, stainless steel, or titanium for metal applications. This powdered material is uniformly distributed across the build platform. Subsequently, the layer-by-layer construction is initiated, guided by a computer-generated 3D model of the intended object (Figure 2.3). The SLS machine commences by selectively sintering the initial cross-sectional layer of the object atop the powdered bed. The laser scans the powder surface, inducing heating and fusion of particles in conformity with the specific shape

of the layer. This phase is succeeded by cooling and lowering the bed; upon the completion of a layer, the build platform undergoes incremental descent, usually equivalent to the layer's thickness. A fresh layer of powder is then spread over the previously sintered layer, and the laser selectively sinters the subsequent layer onto the prior one. This iterative process involves successive sintering, bed descent, and addition of a new powder layer, culminating layer by layer until the entire 3D object takes shape. The final phase, post-processing, transpires after the culmination of the printing process. The printed components undergo cooling within the build chamber. Upon cooling, surplus powder is extracted from the printed object, and any utilized support structures are detached (Mazzoli A., 2013).

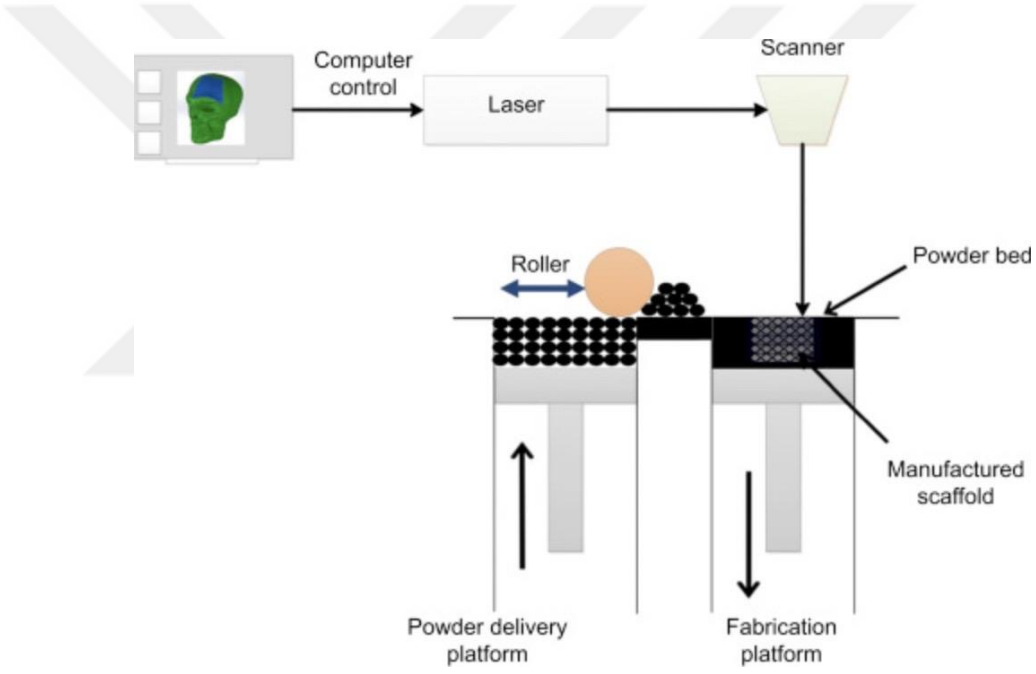


Figure 2.3 SLS Scheme (Munir et al., 2017)

2.1.4. Binder Jetting Method

This represents a technique in additive manufacturing, where objects are constructed layer by layer, employing a binder agent to meld the powder particles together. This method is alternatively recognized as "inkjet 3D printing" or "drop-on-powder printing." The initial stage of the operational mechanism is the preparatory phase, where the process initiates with the creation of a digital 3D model depicting the intended printed object. Subsequently, this model undergoes segmentation into slender layers using specialized software. The subsequent phase is the powder bed, involving

the even dispersion of a thin layer of powder material (such as metal, ceramics, or polymers) across the build platform. The next phase is binder application, wherein a liquid binder is selectively deposited onto the powder layer via an inkjet printhead or a similar mechanism as can be seen inf Figure 2.4. This binder acts as an adhesive, bonding the powder particles together in regions aligning with the cross-section of the object for that specific layer. Post-binder application, the build platform is lowered to accommodate the next layer of powder, and this process is iterated, layer by layer, until the entire object is printed. The application of the binder for each layer follows the defined pattern from the 3D model's segmented data. The final stage involves post-processing, where upon completion of printing, the printed object (still enveloped in excess, unbound powder) is extracted from the build platform. The excess powder can be recycled and used for future prints, making the process more cost-effective. There is an optional step too; Sintering. This one depending on the material used, some binder jetted parts may require additional post-processing steps. For example, metal parts often undergo sintering, a heat treatment process that further fuses the powder particles together, resulting in a more robust and denser final product. There are some advantages of binder jetting method; speed, scalability, material variety and low cost. The limitations of binder jetting method can be listed as follows; surface finish, strength and density. (Ziaee et al., 2019)

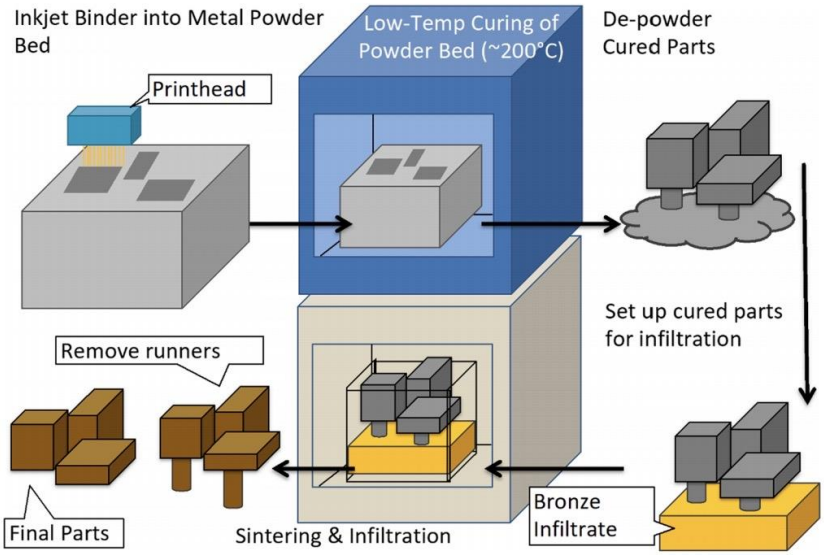


Figure 2.4 Binder Jetting Method Scheme (Mostafaei et al., 2021)

2.1.5. Material Jetting Method

In material jetting, objects are built layer by layer using a printhead that deposits material droplets onto a build platform (Figure 2.5). It is also known as "inkjet 3D printing" because it operates similarly to the way inkjet printers create images on paper. Material jetting process generally includes this steps; digital design, material section, printing process, layer-by-layer building, support structures and post processing. There are some advantages of material jetting; high resolution, multi material printing, wide material section and no need for support molds. Also, there are some limitations of this method; speed, cost and material limitations which means not all materials are suitable for material jetting method. (Gülcan et al., 2021)

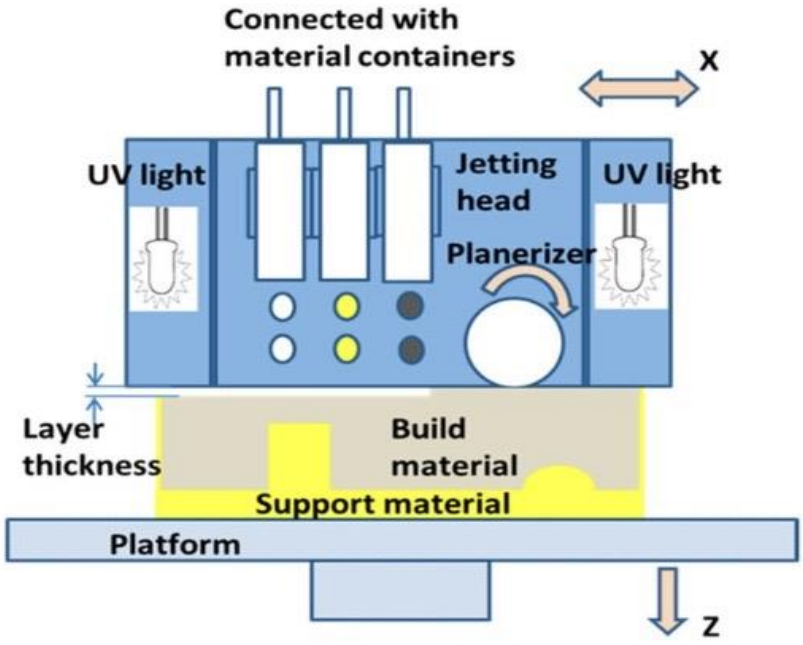


Figure 2.5 Scheme of Material Jetting Method (Yang et al., 2017)

2.1.6. Stereolithography (SLA) and Digital Light Processing (DLP) Method

Liquid photopolymer resin is contained in a raw material reservoir in SLA method. A printing plate is located inside the chamber. Resin is another name for the liquid raw material used in SLA. Resins are made from photosensitive thermoset polymers. The liquid resin's monomer carbon chains are activated by the UV laser's light during photopolymerization and solidify by making robust, irreversible connections with one another. The area contacted by the single point laser installed within the machine

solidifies once the build plate is submerged in the liquid resin. The desired layer is thus produced. The platform rises when the whole cross section of the corresponding layer has been created, allowing the liquid resin to flow underneath this layer. The sections suitable for the cross-section of the object to be made are now solidified by the laser, and they are applied to the preceding layer. DLP 3D printers operate on a similar principle to SLA 3D printers in terms of production. The primary distinction between them is that whereas DLP 3D printers use projectors as their light source, SLA 3D printers employ lasers as their light source as can be seen in Figure 2.6. The projector creates the relevant layer's portion all at once, whereas the laser goes along the relevant layer's section while creating the relevant layer. (Salonitis K., 2014)

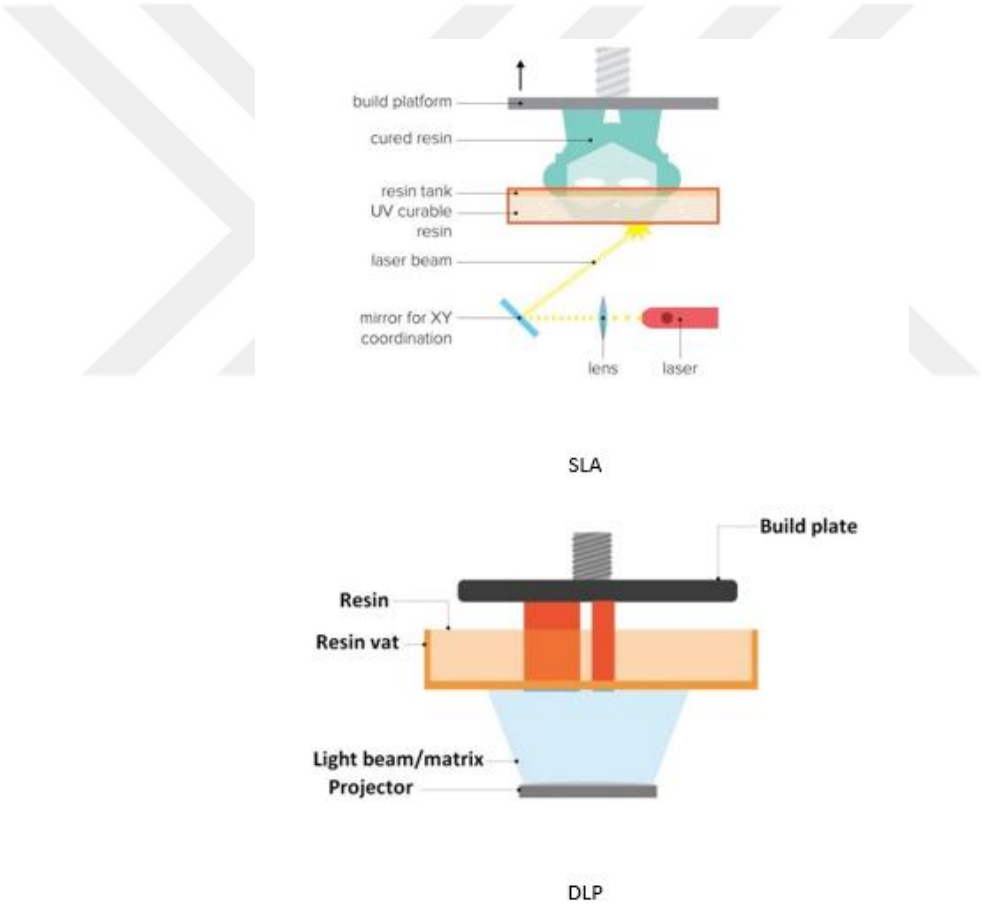


Figure 2.6 SLA and DLP type 3D Printers Schemes (Maines et al., 2021)

2.2 Photosensitive Resin

In three-dimensional printers working with the photochemical principle, light-polymerizable resins are used as building materials. These materials, also known as

photopolymers, are polymers that chemically change under UV light and laser beams. The substance to be generated through this approach comprises photopolymerizable resins, encompassing monomers, oligomers, photoinitiators, and optionally incorporated nanoparticles and color pigments. Photocurable resins are light-sensitive polymer-based materials that change their properties when exposed to UV light. The monomer and oligomer compositions in the photocurable resins determine the mechanical properties (strength, hardness, shrinkage rate, viscosity). To eliminate this effect, diluent monomers that provide flexibility can be added to monomers with high viscosity and thus strength values. These flexible diluent monomers are generally long-chain monomers with low viscosity, low glass transition temperature, and high shrinkage rates. When this monomer mixture is exposed to light of appropriate wavelength with the help of photoinitiators added to the reaction vessel, they form cross-links and bond to each other and the targeted polymer is obtained. (Xu et al., 2021)

However, with the developing industry, increasing waste production and therefore feeding the recycling problem. Today, approximately 90% of epoxy thermosets are obtained from epoxy monomers of the bisphenol-A diglycidyl ether type, obtained from the reaction of epichlorohydrin and bisphenol-A in the presence of sodium hydroxide. The fact that epoxy production is almost entirely dependent on fossil resources does not seem suitable for limiting greenhouse gas emissions, and as a result, it causes the effects of global warming to increase. These epoxy resins are neither biobased nor biodegradable, and in this context, they cannot be included under the umbrella of "green engineering", which is on the rise all over the world.

The greening of the global economy, carbon footprint awareness, increasing emphasis on sustainable systems and the evolution of product life cycle analysis have led many thermoset resin manufacturers to produce plant-based resins rather than oil and gas wells. Resin production from corn and soybean oil is on the rise as it is environmentally friendly. A bioresin is a resin that derives some or all of its constituent monomers from biological sources. In this direction, research has been carried out to develop bio-based epoxy thermosets from renewable resources in order to replace petroleum-based epoxy systems. The resulting biobased epoxies stand out because

they have properties comparable to their petroleum-based counterparts and are environmentally friendly.

Many natural oils are used for the production of biobased resins, some of them are; palm, corn, canola and soybean oil. When looking at the literature, it is seen that soybean oil is frequently preferred due to its high conversion rate compared to others. The form of soybean oil used as resin is epoxidized soybean oil. This type of biobased epoxy is a biobased material obtained by epoxidation of soybean oil with hydrogen peroxide (H2O2) and acetic acid (or formic acid), converting the double bonds into epoxy groups that are non-toxic and have higher chemical reactivity.

When looking at the literature; Compared to petroleum-based resins, biobased resins have been shown to have lower mechanical properties. For this reason, they are not frequently preferred in daily life. For example, AESO's poor mechanical and thermal properties due to its three long aliphatic chains reduce the value of this material.

2.2.1. Monomers and Oligomers

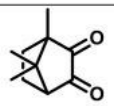
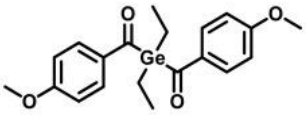
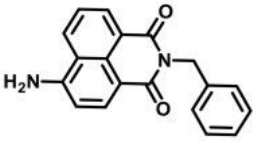
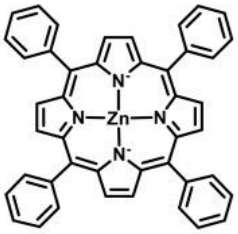
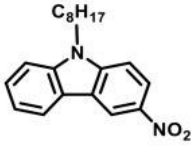
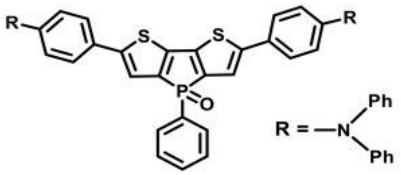
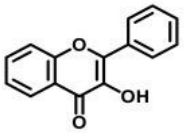
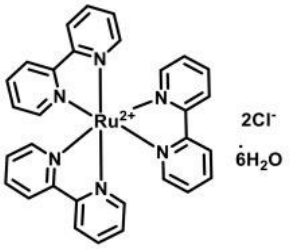
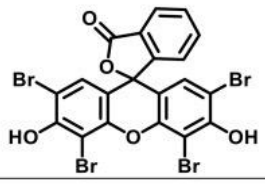
The resin materials used for additive manufacturing in the context of SLA and DLP type 3D printers depend significantly on monomers and oligomers. Small, reactive molecules known as monomers may bond together to form long chains called polymers. Monomers are the building blocks that are utilized to generate the polymer network in the hardened resin in the context of 3D printing resins. The intermediate molecule known as an oligomer is made up of a few monomer repeats. They are smaller than fully formed polymers nevertheless have a larger molecular weight than monomers. (Zhang et al., 2018)

2.2.2. Photoinitiators

Photocurable resins are polymerized with a photoinitiator added to them. The photoinitiator absorbs the light of the appropriate wavelength, and the reagents formed as a result of this absorption allow the monomers in the structure of the resin to cross-link and combine and thus solidify. (Kowalska et al., 2021)

Common photoinitiators and wavelengths are given in Table 2.1 below:

Table 2.1 Common Photoinitiators (Bagheri et al., 2019)

Name	Chemical Structure	Light absorption (λ_{max})
Camphorquinone (CQ)		468 nm
Bis (4-methoxybenzoyl) diethylgermanium (Ivocerin)		408 nm
5-amino-2-benzyl-1H-benzo[de]isoquinoline-1,3(2H)-dione (NDP2)		417 nm
Zinc tetraphenylporphyrin (ZnTPP)		420 nm
3-nitro-9-octyl-9H-carbazole (C2)		375 nm (broad absorption within 350-450 nm)
2,6-bis (triphenylamine) dithieno[3,2-b:2',3'-d] phosphole oxide (TPA-DTP)		465 nm
3-hydroxyflavone (3HF)		λ_{max} = 350 nm (broad absorption within 370-470 nm)
Tris (2,2-bipyridyl) dichlororuthenium (II) hexahydrate (Ru)		453 nm
eosin Y		524 nm

2.2.2.1. Conversion Degree

Monomers, which are small, reactive molecules, react chemically to form long chains of polymers, which are the building blocks of polymer resins. This procedure, called polymerization, can be triggered by a number of factors, including heat, light, or the inclusion of chemical initiators. The proportion of reacted monomers to the total number of monomers in the resin is represented by the conversion degree, which is stated as a percentage. A conversion degree of 80%, for instance, indicates that 80% of the monomers have reacted and polymerized while the other 20% are still in their unreacted state. A crucial factor in determining the final qualities of the cured resin is the degree of cure. While a lower conversion degree could provide a less strong and weaker material, a greater conversion degree often results in a more cross-linked and strong polymer network. As the degree of conversion increases, mechanical properties such as fracture toughness, surface hardness and wear resistance also increase. Monomers that do not react and reduce the conversion rate cause an increase in the shrinkage rate, which leads to a decrease in the hardness and modulus of elasticity. (Chung et al., 1990)

2.2.3. Fillers

Fillers; added to resins to positively affect mechanical properties such as tensile strength, bending strength, hardness, and thermal properties. Fillers can be organic or inorganic, and micro or nano-sized. If the filler added to the resin is in micro size, the composite is formed, if it is in nano size, it is called nanocomposite. The nanoparticles that are generally chosen as filling materials can be listed as follows: cellulosic nanocrystals, cellulosic nanofibers, lignin, silica, zirconia, titania, glass fibers, carbon nanotubes, chitin nanowires. (Shajii et al., 1999)

2.2.3.1 Silica Nanoparticles

Silica nanoparticles attract attention with their high UV absorbance (200-700 nm), bio biocompatibile, positive effect on the degree of conversion and increasing mechanical properties (Guleria and Salhotra, 2016). Silica nanoparticles resist scratching, abrasion, gases and moisture, leading to marked improvements in various

mechanical and electrical properties, including thermal stability and chemical resistance (Cho J. D., et al, 2005).

The properties of materials vary depending on their size; nanosized materials show unique physical and compound properties compared to micro and macro dimensions. Studies have shown that the temperatures of nano-sized pow ders decrease compared to micro-sized powders and that they can be easily confined. This feature is attributed to the fact that nanoparticles provide more atom contact than other particles due to their high surface areas. (Kavaz D., 2022)

2.3 Nanoparticles

Nanoparticles refer to minuscule particles characterized by sizes typically ranging from 1 to 100 nanometers (nm). The dimensions of nanoparticles place them on the scale of individual atoms and molecules, considering that a nanometer constitutes one billionth of a meter. Nanoscale materials encompass various classes, including nanocrystals, nanoparticles, nanotubes, nanowires, nanorods, or nano thin films. These particles exhibit characteristics that are commonly perceived as distinct from and superior to those found in traditional commercial materials. The appeal of frequently cited nanoparticle attributes arises from quantum size effects, the size-dependent nature of electronic structure, unique surface atom features, and the elevated surface/volume ratios. The creation of nanoparticles has contributed to the advancement of various technological and pharmaceutical products. These include powerful catalysts, unique materials used in optical applications, superconductors, anti-wear additives, surfactants, drug delivery systems, and specialized diagnostic tools. Furthermore, the manipulation of nanoscale materials allows the production of compact devices endowed with distinctive capabilities, including high-capacity data storage cells, nanocarriers, sensors, and nanomachines (Liveri, V. T., 2006).

2.3.1. Production Methods

Methods to produce nanoparticles are investigated using the "Bottom Up" and "Top Down" methodologies, respectively. The top-down approach's procedures rely on energizing the volumetric material from the outside using mechanical and/or chemical processes to separate it into little fragments that can be as small as nanometers. The

realization of particle production by increasing atomic or molecular structures with chemical processes is one of the ways included in the bottom-up approach. (Gürmen et al., 2008)

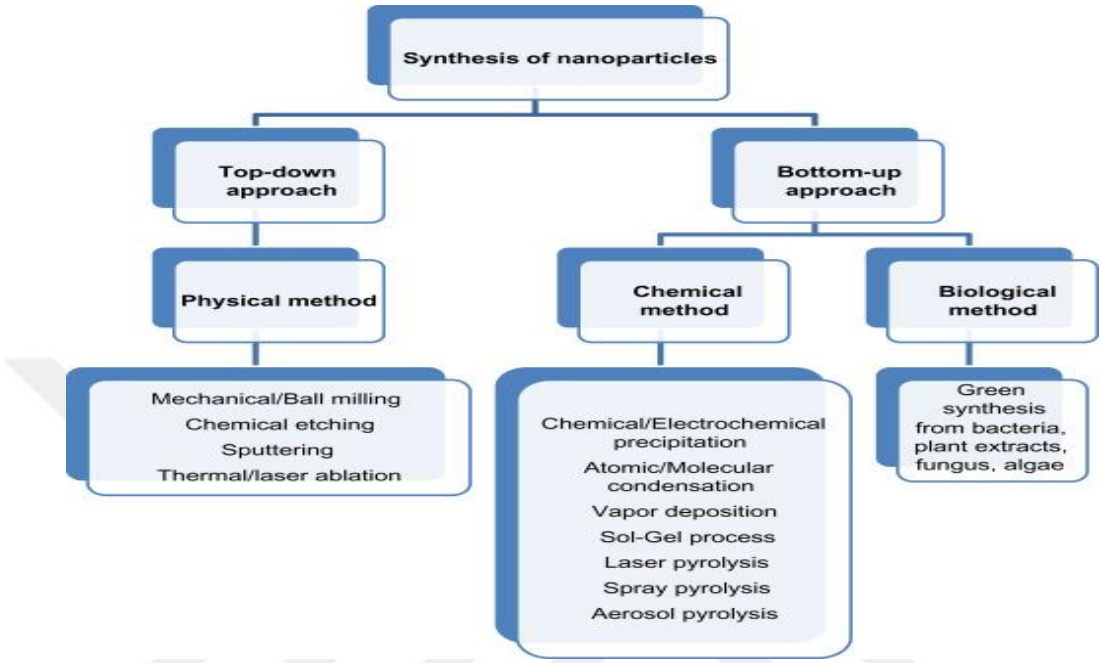


Figure 2.7 Sythesis of Nanoparticles Scheme (Shnoudeh et al., 2019)

2.3.1.1. Sol-Gel Method

The synthesis of many materials, including nanoparticles, thin films, and bulk solids, can be accomplished using the flexible and widely used sol-gel approach. Through chemical processes, a colloidal suspension (sol) is converted into a solid gel network. Due to the flexibility of the sol-gel process, the final product's composition, structure, and properties can be precisely controlled.

Condensation and hydrolysis are the two primary chemical reactions involved in the sol-gel process. The precursor molecules are changed by these processes into a sol and then into a gel form. The steps of the sol-gel method can be listed as follows; hydrolysis, condensation, aging, drying and calcination. The hydrolysis step; The precursor molecules, often metal alkoxides or metal salts, combine with water (H_2O) to produce metal hydroxides or metal alkoxides during the hydrolysis process. Usually, an acid or a base will catalyze this reaction. Considering M as the metal, the hydrolysis reaction can be illustrated as follows:

Metal Alkoxide Hydrolysis:

$$Metal(OR)n + \mathrm{n}H_2\mathrm{O} \rightarrow \mathrm{M(OH)n} + \mathrm{nROH} \quad (2.1)$$

Condensation step; The hydroxide or alkoxide species produced during hydrolysis go through a self-polymerization process in the condensation step, where they interact with one another to create a three-dimensional network of related molecules or particles. Gel is produced as a result of this process. The condensation reaction can be represented as:

Metal Hydroxide Condensation:

$$\mathrm{M(OH)n} \rightarrow \text{Metal Oxide } (\mathrm{M-O-M}) + H_2\mathrm{O} \quad (2.2)$$

Metal Alkoxide Condensation:

$$\mathrm{M(OR)n} \rightarrow \text{Metal Oxide } (\mathrm{M-O-M}) + \mathrm{ROH} \quad (2.3)$$

Aging step; after gelation, the gel may go through an aging process that entails letting the gel sit still for a given amount of time. The gel's structural and mechanical qualities improve with age. Drying; the solvent is eliminated through drying once the proper gel structure has been achieved. Depending on the particular material and its purpose, many drying procedures can be used, such as evaporation, supercritical fluid extraction, or freeze-drying.

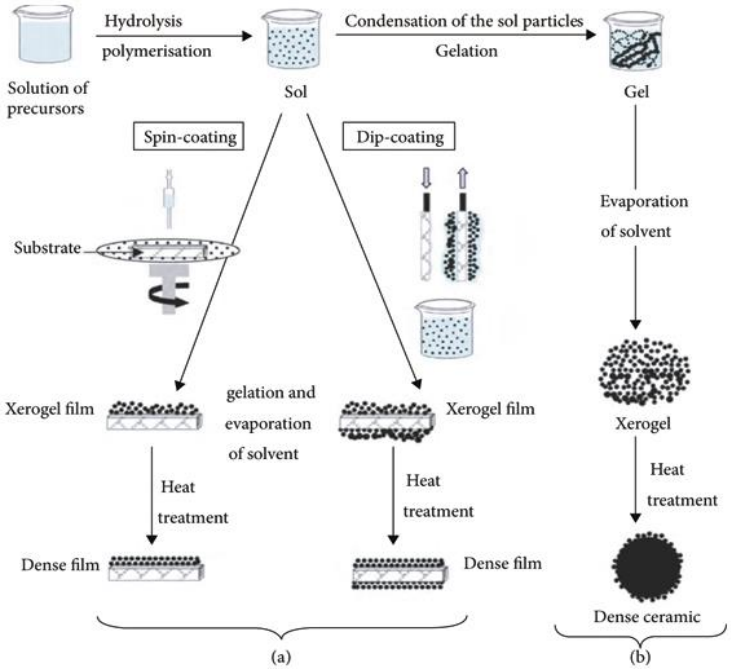


Figure 2.8 Flowchart of Sol-Gel Method (Bokov et al., 2021)

And the last one is calcination; a post-treatment process known as calcination is occasionally used, especially for metal oxide gels. Calcination is the process of heating dried gel at high temperatures to eliminate any organic components still present and to encourage further crystallization and densification of the substance. After this all process, the nanoparticle which desired is produced. There are a few advantages of the sol-gel method; such as chemical composition control, homogeneity, purity and versatility. (Singh et al., 2014)

2.3.2. Silanization

An inorganic substrate, such as glass, silica, metals, or ceramics, is usually employed in the chemical process known as silanization, also known as silane functionalization or silanizing, to change the surface properties of the material. Organosilanes are deposited onto the surface of these materials during the procedure to form a monolayer or thin film of functional groups. Silanization is frequently used to increase the surfaces' wettability, adhesion, reactivity and also prevents agglomeration; making them better suited for use in a variety of industries like surface science, nanotechnology, and biotechnology.

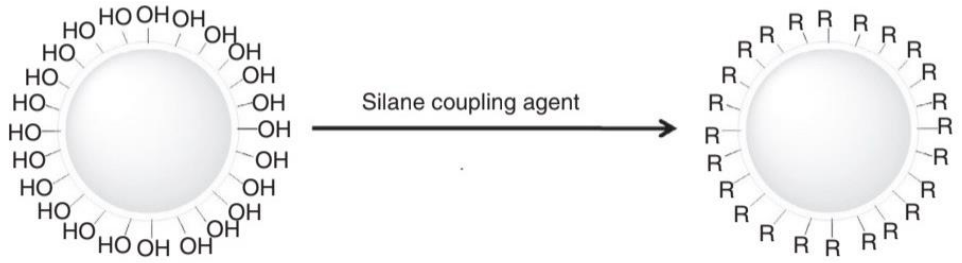


Figure 2.9 Impression of Silanization (Wang et al., 2020)

Trialkoxysilane, serving as a binding agent with silane properties, features dual functional groups located at each end of its molecular chain. These terminal groups establish bonds with both the inorganic substrate and the unreacted resin matrix. The general formula for this dual-functional silane is R-(CH_2)k-Si-$(OR)_3$. In this context, "R" denotes the organofunctional group (such as methacrylate, acrylate, isocyanate, epoxy, etc.), and "-(CH2)-k" represents the linker group strategically positioning the Si atom between the organofunctional group and the linker group. The "OR"

component signifies the activated alkoxy group, specifically methoxy or ethoxy. Prior to binding to the inorganic substrate, the silane undergoes activation with acid (e.g., acetic acid) at room temperature, resulting in the formation of silanol (-SiOH) (Lung et al., 2010).

The hydrolysis process of silanes encompasses multiple chemical stages, with factors such as the molecular structure of the silane, its concentration, pH, temperature, humidity, and the solvent system significantly influencing the speed of silane hydrolysis. Ethanol is commonly incorporated into the solvent system due to the ease of silane solubility in ethanol, while it remains insoluble in water. The hydrolysis rate is impacted by the volume of alkoxy groups, with a decrease in hydrolysis rate corresponding to an increase in the size of alkoxy molecules. pH levels also play a role in silane hydrolysis, with both alkaline and acidic environments accelerating the hydrolysis rate. Furthermore, heat serves as a pivotal factor, with an elevation in temperature correlating with an acceleration in the hydrolysis reaction rate. Upon application to the substrate, the silane undergoes acid activation to generate silanol groups. Between the functional groups of the resin and the silane's organofunctional groups (C=C bond), a reaction occurs. Reactive free radicals are created when reactive radical groups interact with the silane molecule's C=C link or the resin monomer. A new C=C sigma bond is created when these free radicals interact with the silane molecules and the resin monomers. Finally, a silane coupling agent is used to join the substrate surface and composite resin. (Lung et al., 2013)

CHAPTER THREE
LITERATURE REVIEW

3.1 Biobased Nanocomposite Resins for 3D Printing

According to the literature studies in this field, while bio-based oils were used as lubricants at first, it was discovered over time that they are an eco-friendly option for polymers. (Gryglewicz et al., 2013)

According to the literature, soybean oil (also known as epoxidized soybean oil, or ESO) is the primary source of biobased resins. Which is a green alternative to traditional resins. This kind of biobased epoxy is created by epoxidizing soybean oil with hydrogen peroxide (H_2O_2) and acetic acid (or formic acid), which transforms double bonds into epoxy groups that are non-toxic and have increased chemical reactivity. (Mustapha et al., 2019)

The ring-opening polymerization process is the one recommended most frequently in the literature for an epoxy made from soybean oil. Acetals, esters, amides, and siloxanes all undergo ring opening polymerization with cyclic ether. Ionic and molecular catalysts can start polymerization. Here is an illustration of how ESO is made:

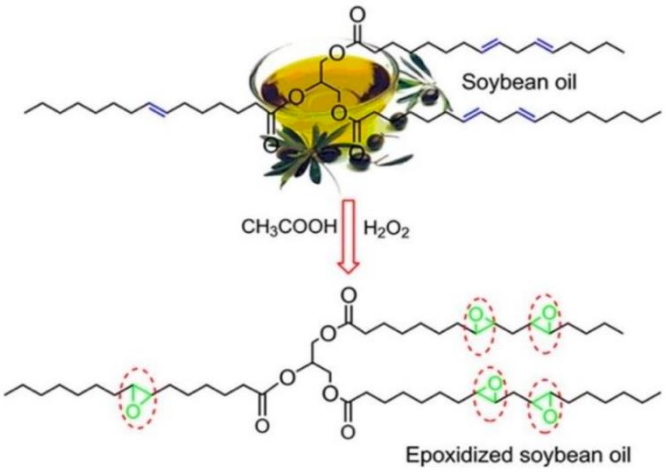


Figure 3.1 Production of ESO (Guit et al., 2020)

Epoxidized soybean oil must additionally go through the acrylate process in order to produce additives with high productivity. Epoxidized soybean oil and acrylic acid react to produce acrylic epoxidized soybean oil (AESO).

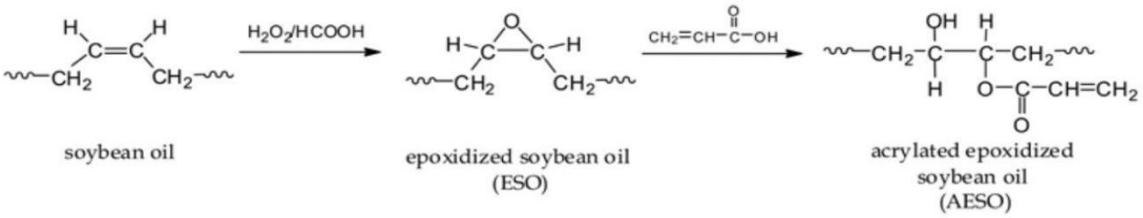


Figure 3.2 Synthesis of AESO (Shibata, M., 2011)

For AESO to be curable and usable in 3D printing technologies, it must have an appropriate viscosity. Diluents are needed to reduce the viscosity value, which is 3.8 Pa.s at room temperature. (Bonnaillie, L. M. 2004)

To reduce the viscosity, diluents such as 1,6-hexanediol diacrylate (HDDA), triethylene glycol dimethacrylate (TEGDMA) and tetrahydrofurfuryl methacrylate (THFMA) are used. One of the diluents frequently used with AESO is TEGDMA, which has a low molecular weight (286.32 g/mol). (Jagtap et al., 2022)

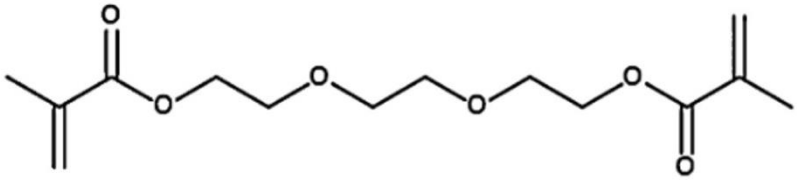


Figure 3. 3 TEGDMA Chain Structure (Jagtap et al., 2022)

A high degree of conversion is required for high mechanical properties. It is known that AESO can achieve high conversion degrees. (Åkesson et al., 2010)

In order to determine the conversion rate, three different calculations can be made with the data from the FTIR analysis. (Barszczewska-Rybarek I. M., 2012)

The following formula is used to determine the conversion rates of aromatic rings:

$$DC_{Ar} = 1 - \left[\frac{\frac{A_{C=C}}{A_{Ar_{polymer}}}}{\frac{A_{C=C}}{A_{Ar_{monomer}}}}\right] \quad (3.1)$$

The value denoted A represents the absorption peak at 1598 cm^{-1} and the value denoted AC represents the absorption peak at 1637 cm^{-1} (Barszczewska‑Rybarek I. M., 2012).

The following formula is used to determine the conversion rate of C=O bonds:

$$DC_{C=O} = 1 - [\frac{\frac{A_{C=C}}{A_{C=O_{polymer}}}}{\frac{A_{C=C}}{A_{C=O_{monomer)}}}}] \quad (3.2)$$

$A_{C=C}$ represents the absorption value at the peak of 1637 cm^{-1}, $A_{C=O}$ at the peak of 1718 cm^{-1}.

The conversion rate in C=C bonds is determined by the formula:

$$DC_{C=C} = 1 - (A_{C=C(t)})/(A_{C=C(0)}) \quad (3.3)$$

$A_{C=C(0)}$ is the value of the absorption peak in 1637 cm^{-1}, and $A_{C=C(t)}$ is the value of the absorption peak in 1718 cm^{-1} (Yang D. L., et al., 2020).

According to the literature, it is seen that the nanoparticle reinforcements made to the resins have a positive effect on their properties. (Palucci et al., 2021)

In the studies carried out in this field, it has been seen that nanoparticle additives can be made successfully and these additives affect the optical, thermal and mechanical properties. Weng Z. et al added silica nanoparticles in different compositions to the resin and obtained three different nanocomposites. They found that the addition of nanoparticles increased the modulus of elasticity and tensile strength. (Yang et al., 2022)

Table 3.1 shows some of the photocurable nanocomposite resin studies encountered in the literature.

Table 3.1 Literature Review

Resin Content	**Filler Material**	**Reference**
AESO	Nanolignin	(Thielemans et al., 2001)
AESO	Nanocellulose	(Palucci et al., 2022)
HEMA-PEGDA	Nano SiO_2	(Liu et al., 2018)
HDDA-TMPTMA	Nano SiO_2	(Zhang et al., 2015)
BEF-EP	Nano diatomite	(Li et al., 2021)
AESO	Wood Fibers	(Quirino et al., 2012)
DGEBA	Nano SiO_2	(Sprenger S., 2020)

In the study of Rosso et al., it was observed that the nano SiO_2 additive made to the epoxy decreased the glass transition temperature, increased the stiffness and toughness, and made it more ductile. (Rosso et al., 2006)

Mahrholz et al. analyzed the mechanical properties of SiO_2 added nanocomposite resin in their study. They noted an increase in the elastic modulus, accompanied by a marginal decrease in the flexural modulus. (Mahrholz et al., 2005)

In another study, Sarac et al., according to the tensile test and dynamic mechanical analysis results, although the mechanical strength of the composites increased with increasing silica concentration, a decrease in the thermal stability (storage and loss modulus) was observed. (Sarac et al., 2019)

CHAPTER FOUR
EXPERIMENTAL STUDIES

4.1 Purpose

Today, it is seen that 3D printers are in demand and are developing day by day. The materials printed on these devices are used in many areas, including daily life. Contrary to traditional epoxy resins, the use of bio-based resins produced under the roof of green engineering is important both in terms of human health and not to harm the ecology. In the literature research, it has been determined that bio-based resins are used in three-dimensional printers, but it has been observed that they are not studied as nanocomposites with nanoparticle additives. In the light of the information obtained here, SiO_2 nanoparticles were added to the biobased resin obtained from AESO and a nanocomposite was obtained for use in three-dimensional printers. The used SiO_2 nanoparticles were produced by sol-gel method and with high purity starting materials. Afterwards, the mechanical properties, organic bond structures, morphological structures, structural and chemical properties of the nanocomposites obtained by adding these nanoparticles, which were subjected to the silanization process, were characterized.

4.2 Materials

This portion outlines the resin employed for nanocomposite manufacturing, the chemicals utilized in nanoparticle production, and surface modification. The biobased resin derived from acrylated epoxidized soybean oil was procured from the AnyCubic company. Tetraethyl Orthosilicate (TEOS), Ammonia, and 3-(Trimethoxysilyl) propyl methacrylate (MPS) were acquired from Sigma Aldrich. Ethanol (EtOH) and Isopropanol (IPA) were obtained from ISOLAB.

4.3 Methods

The studies carried out within the scope of this thesis are listed as the production of nanoparticles, surface modifications (silanization) of nanoparticles and the production of nanocomposite resins containing SiO_2 in different compositions. All of the

experimental studies are shown in the flow chart (Figure 4.1). Each sample was given the aforementioned characterizations.

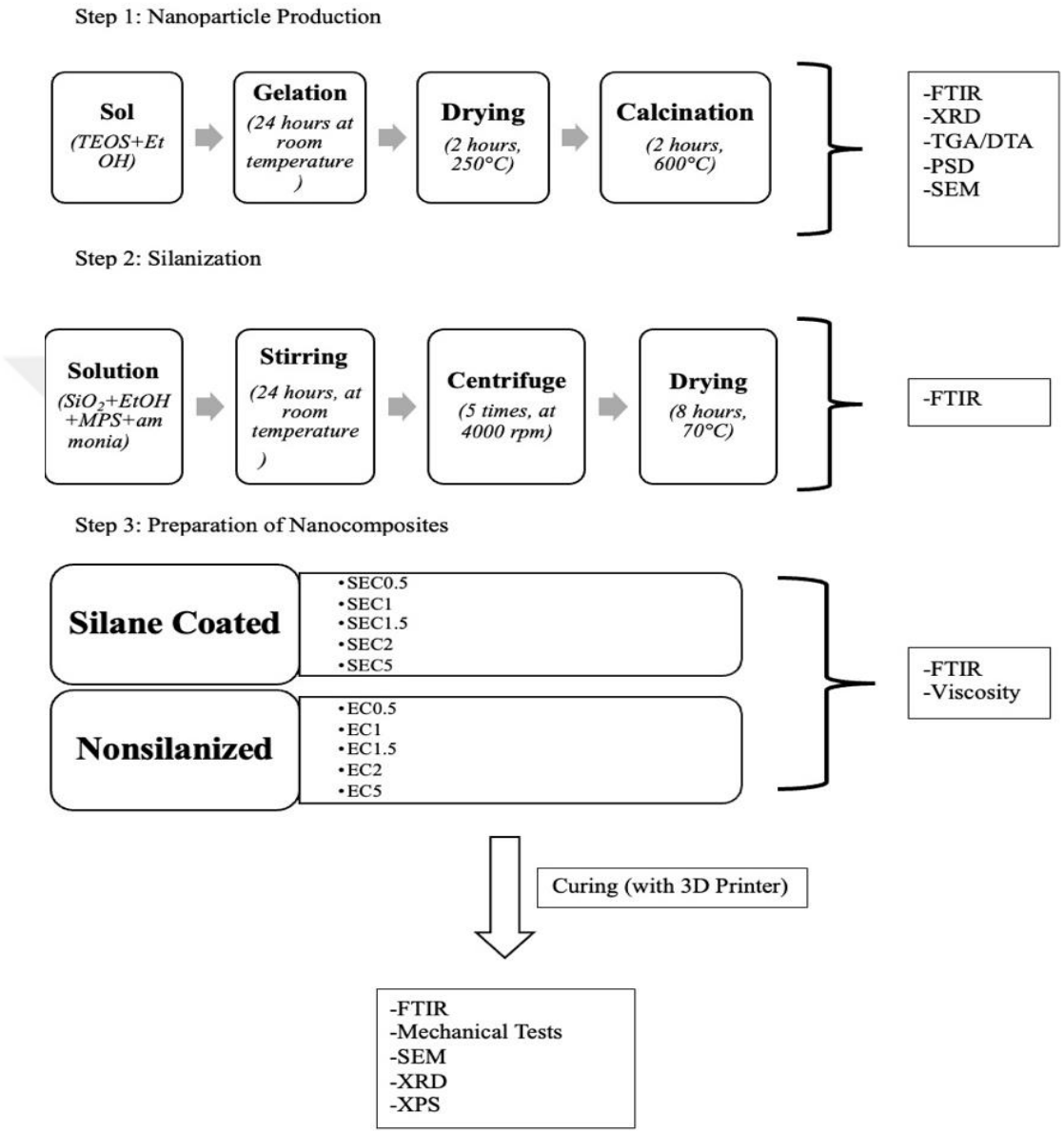


Figure 4.1 Process Scheme of Synthesis and Analysis

4.3.1. Synthesis of Nanoparticles

The synthesis of SiO_2 nanoparticles was executed through the sol-gel approach. The initial phase, sol formulation, involved the utilization of TEOS (Tetraethyl Orthosilicate) and EtOH (ethanol). In a beaker, 4.5 mL of TEOS was introduced to 40 mL of ethanol, ensuring protection from air exposure. The resultant solution

underwent stirring on a magnetic stirrer for approximately two hours until achieving transparency. To this clarified solution, 3 mL of 25% ammonia was incorporated. Following a two-hour magnetic stirring for homogeneity, the solution was left to age overnight at room temperature. The resulting gel underwent TG-DTA analysis to ascertain the calcination temperature. Post-thermal analysis, the gel was subjected to a two-hour drying at 250 °C, followed by calcination at 600 °C for an additional two hours.

The subsequent phase involved the silanization of SiO_2 nanoparticles using MPS (3-(trimethoxysilyl) propylmethacrylate). Initially, 10 g of SiO_2 nanoparticles were dispersed in 250 mL of ethanol. Subsequently, a solution composed of 13 g of water, 6.8 g of 25% ammonia, and 6.2 g of MPS was added to the dispersion. The resulting mixture underwent initial stirring in an ultrasonic bath for thirty minutes, followed by continuous stirring with a magnetic stirrer at room temperature for 24 hours. This mixture, subjected to centrifugation at 4000 rpm, underwent repeated washing with ethanol after each step, involving four additional centrifugation cycles. The acquired nanoparticles were subjected to drying at 70°C for 8 hours, culminating in the completion of the silanization process.

4.3.2. Preparing Samples

These nanoparticles, whose production and surface modifications were carried out, were mixed into biobased resin in different compositions to create liquid samples.The names of the nanocomposite samples containing powders with and without silane in different compositions are given in the Table 4.1.

Table 4.1 Contents and nomenclature of composite resins

Name	SiO_2 (wt %)	Silanized SiO_2 (wt %)
EC	0	0
EC0.5	0.5	0
EC1	1	0
EC1.5	1.5	0
EC2	2	0
EC5	5	0
SEC0.5	0	0.5
SEC1	0	1
SEC1.5	0	1.5
SEC2	0	2
SEC5	0	5

4.3.3 3D Printing

Creality Halot-Sky CL89 (Figure 4.2a), a DLP type printer, was used to print bending and tensile samples. Printing was carried out with a 405 nm UV light source, with a first layer thickness of 50 µm. The exposure time of the first four layers was set to 60 seconds, and the exposure time of the remaining layers was set to five seconds. Then, each printed sample was transferred to the Creality UW-02 Curing and Washing Machine (Figure 4.2b) and washed in IPA for 10 minutes, followed by post-curing for one hour. These processes were performed to removing the uncured monomers remaining in the structure.



a **b**

Figure 4.2 3D printer (a) and curing/washing machine (b)

With these prepared nanocomposites, how the silanization process affects the aggregation amount of the SiO_2 powders in the resin and their distribution in the resin were examined. Then, the optimum number of nanoparticles providing the highest conversion rate and the highest mechanical properties was determined. Finally, the effects of the additive on the structure were investigated in the nanocomposite resins obtained with the determined nanoparticle amounts. Upon examination of Figure 4.3, it becomes evident that the designs for tensile and bending samples, each with a thickness of 3 mm, have been meticulously prepared in compliance with ASTM D638 and D790 standards, as illustrated through their three-dimensional representations.

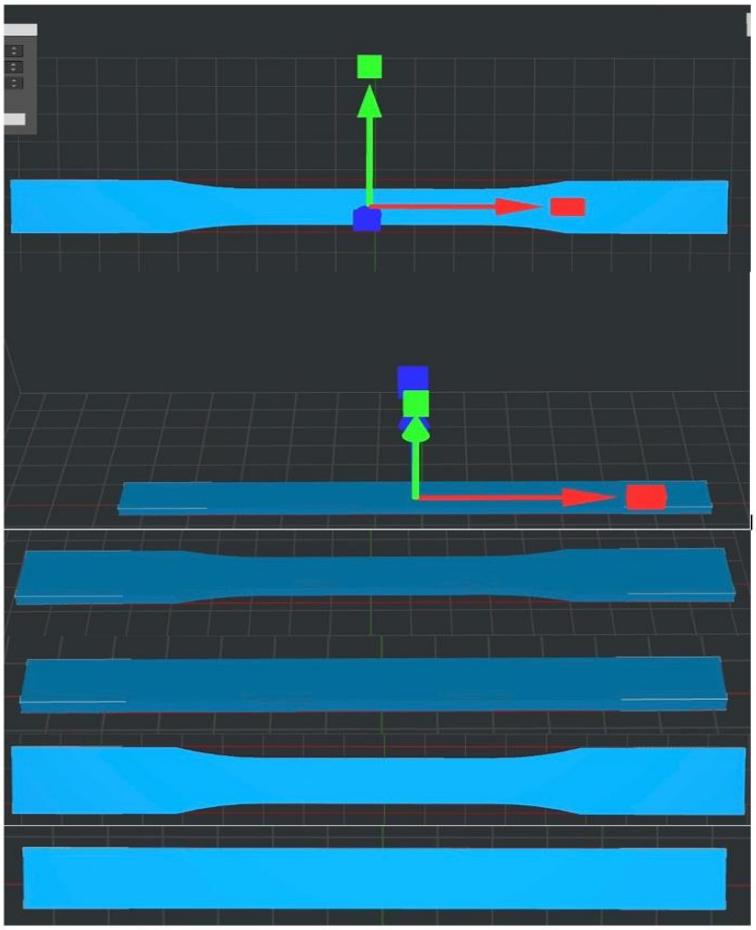


Figure 4.3 3D printer (a) and curing/washing machine (b)

4.4 Characterization

4.4.1 Scanning Electron Microscopy (SEM)

SEM is a particular kind of microscope that provides data on the surface morphology of the substance being examined. The column, vacuum pump, sample holder, and imaging system are the four essential components of a SEM (Fig 4.4). When a tungsten filament is placed inside of a vacuumized tube and subjected to an extremely high voltage, primary electrons are created. This heats the electron beam at the top of the column. Vacuum pumps are used to remove the air in the path of the electrons since the electrons cannot move through air without colliding with air molecules. The main electrons are focused and dropped on the sample as they move through the vacuum with the aid of magnetic lenses after being accelerated by the anode in the center of the column.

The scanning coil hovers this focused beam of electrons over the area of the sample being examined. Auger electrons, secondary electrons (SE), backscattered electrons (BSE) and X-rays are formed as a result of the collision of the primary electron beam with the sample surface. If electrons collide with atoms of large atomic number, light regions will be formed, and if atoms with small atomic number collide, dark regions will be formed. To detect these atoms, a backscattered electron (BSE) detector is required.

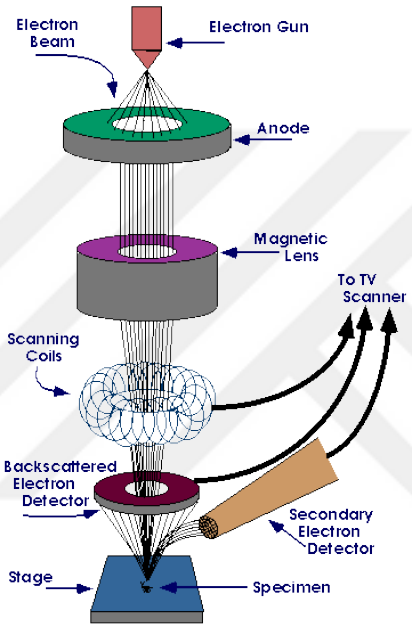


Figure 4.4 Scheme of SEM (Siek M. M., 2016)

In this thesis, the distribution of nanoparticles in the composite and the surface morphology were determined by scanning electron microscope (Fig 4.4). Secondary electron (SE) mode was used to determine the surface morphology, at the 5 kV voltage value. The back scattered (BSE) mode was used to observe the distribution of nanoparticles in the composites, at 15 kV voltage value. The magnification values used in the analysis are as follows; 5K, 10K, 25K, 50K and 100K.

4.4.2 X-Ray Diffraction (XRD)

X-ray diffraction (XRD) stands as a commonly employed analytical approach for acquiring insights into the crystal structure and phases of a material (Fig 4.5). The X-Ray Diffraction technique (XRD) operates on the premise that each crystal disperses

X-rays in a distinct pattern, contingent upon the distinctive atomic configuration of the phase (Fig 4.5). The diffraction profiles associated with each crystal phase serve as a unique identifier for that crystal, akin to a fingerprint. This underlying principle is also fundamental to Bragg's law, which serves as the primary tenet of X-Ray analysis.

$$n\lambda = 2dsin\theta \tag{4.1}$$

"λ" is standing for the wavelength of the x-ray and "θ" is standing for the angle between the incident ray and the scattering plane, "d" represents the distance between the crystal layers, "n" is an integer. By looking at the graph obtained as a result of the analysis made by using this method, the crystal structure of the material and its phase are observed.

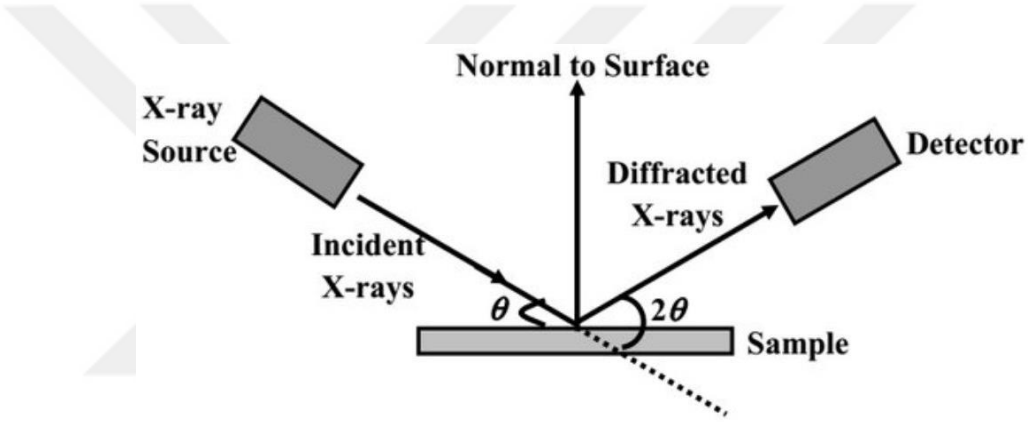


Figure 4.5 XRD Device's Working principle (Wubet W., 2019)

This thesis employs XRD analysis (Thermo Scientific ARL X'TRA) to ascertain the phase and crystal structures of SiO_2 nanoparticles and nanocomposites. The X-ray diffraction measurement utilizes Cu-Kα radiation (wavelength of 1.5406 Å), with diffraction patterns generated to determine the 2θ value. Data collection occurs at a scan rate of 2°/min within the $20° \leq 2\theta \leq 80°$ range.

4.4.3 Fourier Transform Infrared Spectroscopy (FT-IR)

IR spectroscopy facilitates the molecular-level examination of materials by exploiting the distinct frequency values generated through the vibrations induced by the IR beam on molecules (Fig. 4.6). The variations in bond angle and length contribute to diverse vibration patterns, and these distinctions are evident in the frequency values. Fourier transform (FT) is a mathematical operation, which converts

the time series representation of a signal function into a frequency spectrum that can be analyzed mathematically by some algorithms. IR light is sent to the sample to obtain an IR spectrum. For a molecule to absorb IR light, there must be a net change in the natural dipole moment of the molecule as a result of the vibration of the molecule. It is checked how much of the transmitted light is absorbed at a certain energy. The energy at which a signal (band) is obtained in the absorption spectrum gives the vibrational frequency of the sample molecule. Since information is obtained directly at the atomic level with FT-IR, even very small changes in molecules can be detected. When certain molecules are exposed to infrared light, they are characterized by molecular bond vibration signals that they give at certain frequencies (cm^{-1}). The change in different conditions over these signals can be easily monitored with FT-IR.

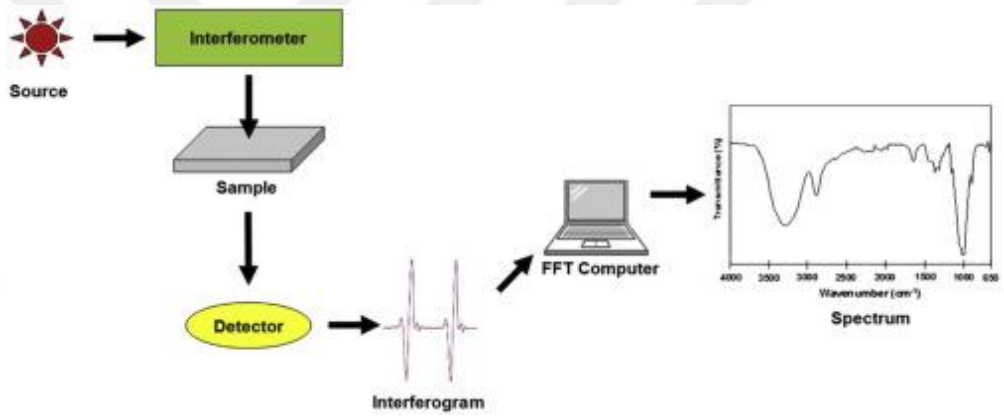


Figure 4.6 Working Principle of FT-IR (Undavalli et al., 2021)

Within the scope of this thesis, the success of the silanization process applied to SiO_2 nanoparticles and the conversion degrees of the obtained nanocomposites were observed using Fourier Transform Infrared Spectroscopy (Thermo Scientific NICOLET iS10). In this analysis, absorption spectra were obtained in the wavelength range of 4000 cm^{-1} to 500 cm^{-1} by scanning each sample 20 times.

4.4.4 X-Ray Photoelectron Spectroscopy (XPS)

This apparatus is designed to analyze the elemental composition, empirical formula, and chemical and electronic states of a given material. While X-rays are sent to the material with the XPS device (Fig 4.7), the kinetic energy of the surface of the material at a depth of 1 to 10 nm and the number of electrons ejected from the surface are

measured. XPS detects atomic number 3 (lithium) and higher. Since the orbital diameters are small, it cannot detect hydrogen atoms with atomic number 1 and helium atoms with atomic number 2. XPS is a surface analysis method. It is based on the logic of excitation of electrons in the energy levels of the inner shells (core level) of surface atoms as a result of photoelectric effect (Moulder et al., 1992).

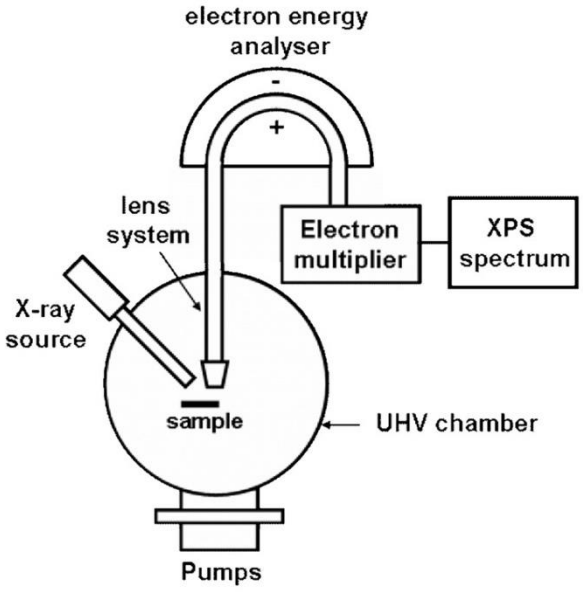


Figure 4.7 XPS Scheme (Regonini D., 2008)

If the kinetic energies of the electrons excited with a certain energy due to the photoelectric effect are known, the binding energies can also be calculated. The binding energy gives us information about the atoms on the surface, the valence of these atoms and their chemical structures.

In this thesis, the elemental contents of nanocomposites were determined by x-ray photoelectron spectroscopy analysis (Thermo Scientific K-Alpha). In this measurement, monochromatic Al-Kα (1486.7 eV) with 400 μm diameter beam were used as x-ray source. XPS scanning was performed with a pass energy of 150 eV from -10 to 1350 eV and using a scanning rate of 1 eV. Elemental scanning was performed with a scanning rate of 0.1 eV, applying a transition energy of 30 eV. Samples were scanned 10 times for elemental data.

4.4.5 Particle Size Distribution (PSD)

Particle size distribution analysis provides data on the sizes of particles. The dynamic light scattering technique was utilized to observe the size and distribution of nanoparticles by Particle Size Distribution Measurement (Malvern, Zeta Sizer Nano ZS90). In this method, a suitable solvent is found for each material, the particles whose size is desired to be determined are dispersed in the appropriate solvent and the analysis is carried out in a light-permeable tube. As a result of the analysis, the sizes and size distribution percentages of the measured particles are obtained.

Within the scope of this thesis, SiO_2 nanoparticles were dissolved in isopropyl alcohol by ultrasonic bath and particle size distribution analysis was performed at room temperature. The average of ten measurements was taken for the baseline result.

4.4.6 Thermogravimetric and Differential Thermal Analysis (TG/DTA)

Thermogravimetric analysis (TG) is a method providing measurable alterations in the mass of a specimen due to rising temperatures. It allows the observation of mass variations during substance dehydration or degradation based on time or temperature. Weight modification ensues from the disruption of physical or chemical bonds at elevated temperatures. The Differential Thermal Analysis (DTA) method scrutinizes the temperature variance between the sample and reference material relative to the applied temperature. Its broader applicability stems from not being solely reliant on mass loss, as observed in TGA. It can be applied to any sample where heat is absorbed or released. One of the important uses of DTA is the creation of phase diagrams in studies related to phase transitions.

Within the scope of this thesis, TG/DTA analysis was performed to determine the thermal properties and the phase transformation behaviors of the materials and their decomposition behavior according to the temperatures were determined. When the data from these analyzes are examined together, how the mass loss changes with temperature and the reactions that occur with it are observed.

TG/DTA (PerkinElmer, STA8000) analysis was performed in a nitrogen atmosphere, in the range of 0 – 1000 °C and with a rise rate of 5 °C/min.

4.4.7 Viscometer

The flow and deformation behavior of materials can be measured and examined using a rheometer, a specialized instrument. It is used to determine the rheological properties of the material when the viscometer alone is not sufficient, it can also act as a viscometer for liquids. Therefore, it was used in this thesis to measure the viscosity of resins.

To evaluate the suitability of the prepared resins for 3D printing, their viscosities were measured using a rheometer (Bohlin Instruments CVO Rheometer System) utilizing the cone and plate technique. The distance between the two plates was established at 100 μm, and the cone angle was set at 2°. Measurements were carried out for a duration of 120 seconds, covering a range of shear rates from 0 to 1000 (1/s), with one measurement per second.

4.4.8 Mechanical Tests

Mechanical tests are crucial operations carried out on materials to evaluate their mechanical properties, behavior, and reaction to different forces and conditions. By giving insightful information about the performance, reliability and durability of materials, these tests play a crucial role in the material science, engineering, and manufacturing industries.

Mechanical assessment employs a range of robustness examinations to evaluate the appropriateness of a material or component for its designated usage. These tests gauge characteristics like pliability, tensile strength, elongation, hardness, toughness, impact resistance, stress fracture, and the modulus of elasticity. Common mechanical examinations utilized in analyses encompass breaking strength, bending, shear strength, impact, and hardness assessments. Within the scope of this thesis, three-point bending test and tensile test were applied to determine the modulus of elasticity and to calculate the yield and bending strength.

4.4.8.1 Three Point Bending Test

Bending test is the deformation that occurs when a constant directional force is applied to the middle of a sample, usually of circular or rectangular cross-section, which is placed between two supports, at equal distance to both sides.

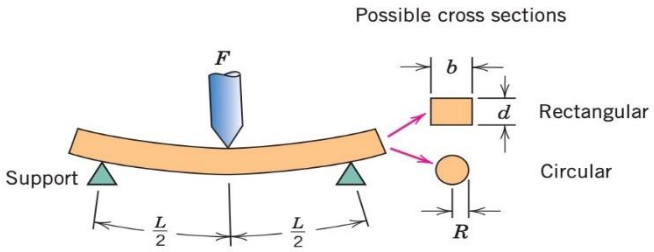


Figure 4.8 Scheme of Three Point Bending Test (Callister & Rethwisch, 2018)

In this thesis, the bending strength of the acquired nanocomposite samples was ascertained through a three-point bending test conducted at a rate of 2 mm/min, employing a Shimadzu AG-50kNG apparatus in strict adherence to ASTM D790 standards. The spacing between the supports was determined as 50 mm. Calculations were made in accordance with the following Equation 4.2 by utilizing the applied load up to the fracture.

$$\sigma_{fs} = \frac{3*F_f*L}{2*b*d^2} \tag{4.2}$$

The representations in the formula are as follows; "σ" for flexural strength, "F" for load at break, "L" for span distance, "b" for sample width and "d" for thickness.

4.4.8.2 Tensile Test

The objective of the tensile examination is to assess the static load-induced elastic and plastic characteristics of materials. The tensile testing apparatus comprises two adjustable grips along the z-axis, where the specimen is affixed, and components that impart force to them while measuring these two parameters. By consistently moving the load cell, different degrees of tensile force are exerted on the specimen, and the corresponding elongation is documented. An extensometer is employed to record the sample's deformation during the application of force.

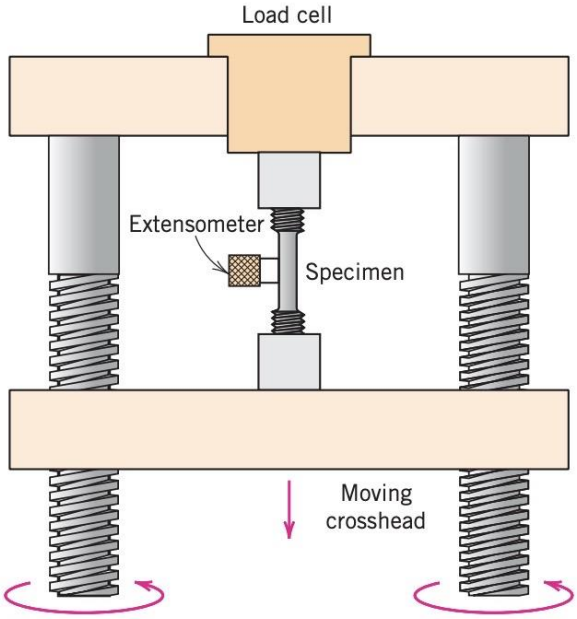


Figure 4.9 Tensile Test Scheme (Callister & Rethwisch, 2018)

The modulus of elasticity and yield strength of the samples were determined by a tensile device which named Shimadzu AG-IS (Fig. 4.9) and pulling the grips at a speed of 1 mm/min according to ASTM D638 test standard. Engineering stress and engineering strain are calculated with the data obtained from this characterization. The formula Equation 4.3 used to determine engineering stress is as follows:

$$\sigma = \frac{F}{A_0} \tag{4.3}$$

"F" represents instantaneous load, "σ" represents instantaneous stress and "A_0" represents the cross-sectional area. Engineering strain is obtained with the following Equation 4.4:

$$\varepsilon = \frac{l - l_0}{l_0} \tag{4.4}$$

The engineering strain represented by "ε", the "l_0" is the length before any load was applied and the "l" is the instantaneous length.

4.4.9. Hardness Test

One of the analyzes performed to obtain information about the suitability and durability of the material for its intended use is the hardness test.



Figure 4.10 Shore D test device

Within the scope of this thesis, Shor D test was applied to the samples (Fig. 4.10). This method of analysis is frequently used for materials such as elastomers. This measurement is made with a hardness meter device. The cone-shaped needle at the tip of this device is inserted into the material and as a result of this pressure, a hardness value is read from the indicator on the device.

CHAPTER FIVE
RESULTS AND DISCUSSION

5.1 Characterization of Nanoparticles

5.1.1 Structural Properties

Figure 5.1 presents XRD pattern of the SiO_2 nanoparticles crafted in the synthesis process. The peak seen in the XRD spectra is the characteristic SiO_2 peak. The prevailing peak evident in the analysis implies that the formed SiO_2 particles lack a crystalline arrangement, signifying their existence in an amorphous state. Additionally, the lack of extra peaks in the pattern points to the removal of any lingering organic and salt compounds potentially originating from the synthesis process (Gorji B. et al., 2012).

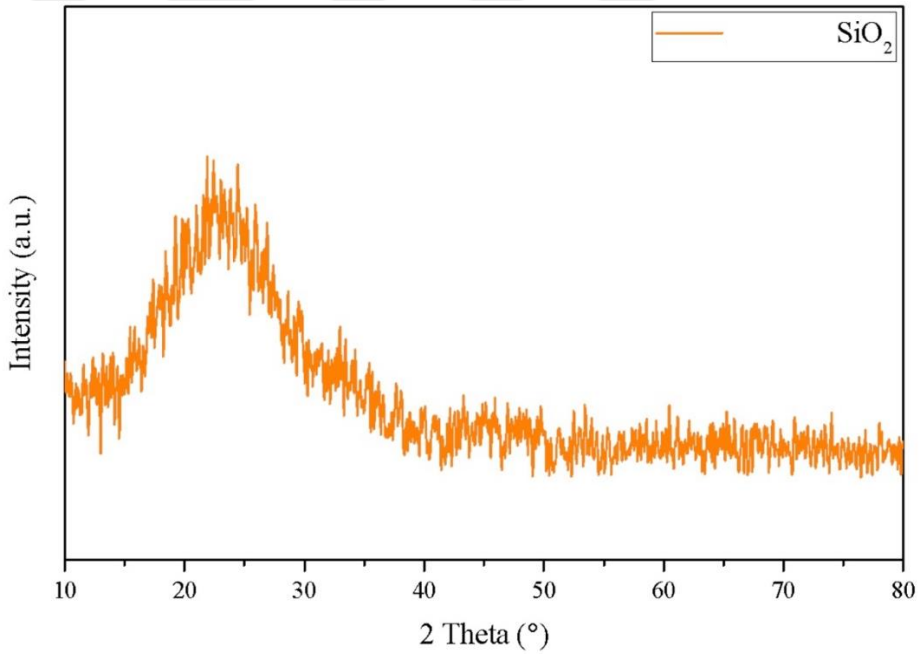


Figure 5.1 XRD Spectra of SiO_2 Nanoparticles

5.1.2 Thermal Properties

TG/DTA analysis was used to observe the changing properties of the produced nanoparticles depending on heat. This assessment was performed on the matured SiO_2 gel, and the ensuing drying and calcination procedures were guided by the outcomes

acquired. Figure 5.2 visually illustrates the temperature-related weight loss and heat flow for the generated SiO_2 xerogel.

Looking at Figure 5.2, the endothermic peak seen around 70 °C represents the dehydration process. When we look at the exothermic peak between 160°C and 360°C, Jafarzadeh et al. as in their work, it is observed that organic components and especially alkyl groups are burned. Looking at the peak at 600 °C, the endothermic peak here is shown as evidence of OH groups leaving the silanol. During this analysis process, no structural phase change was observed (Jafarzadeh et al., 2009). When looking at the weight loss, it is known that there is a loss of approximately 16-17%, and this is thought to be due to the separation of organics.

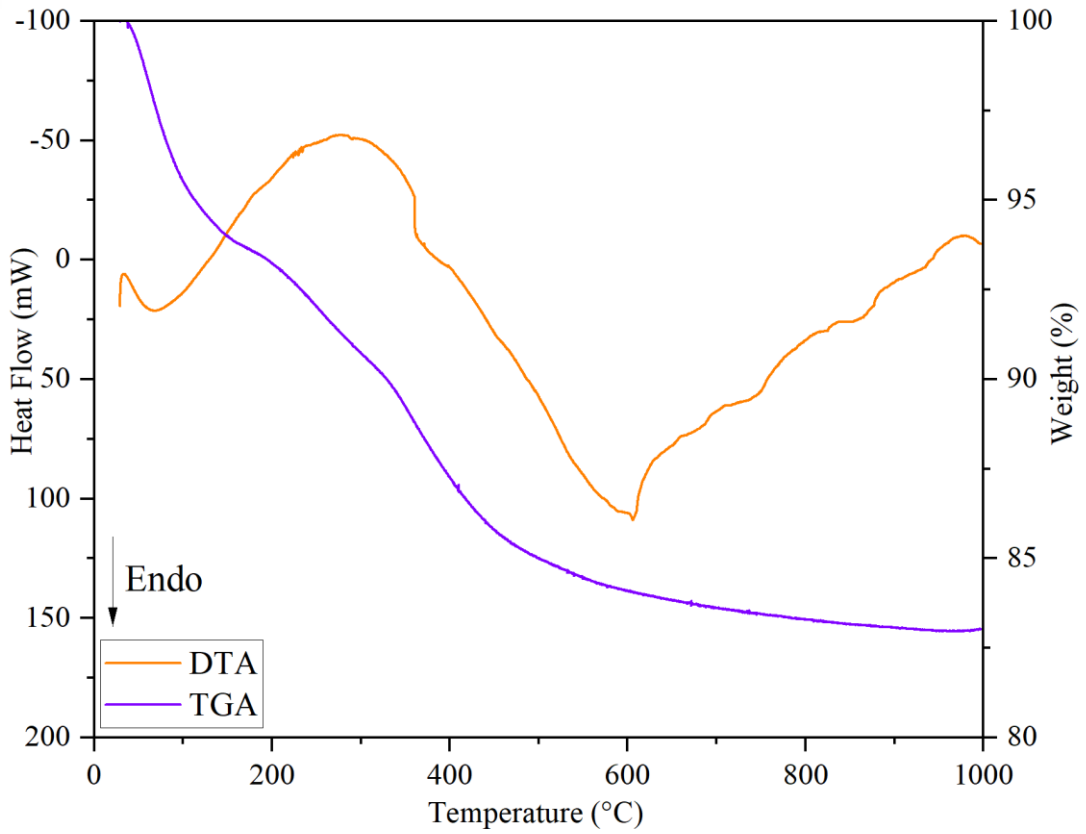


Figure 5.2 TG/DTA analysis of SiO_2 Nanoparticles

5.1.3 Morphological Properties

Using scanning electron microscope (SEM), the morphological properties of SiO_2 nanoparticles were determined and this analysis was carried out in secondary electron mode. The resultant images are depicted in Figure 5.3. The examination of the

nanoparticles' shape and size through SEM analysis took place before the silanization process. When SEM images were examined, the presence of particles that appeared larger due to agglomeration was observed. The sizes of SiO_2 particles in the images are randomly distributed between 40 and 100 nm. These particles appear to be nanosized and spherical.

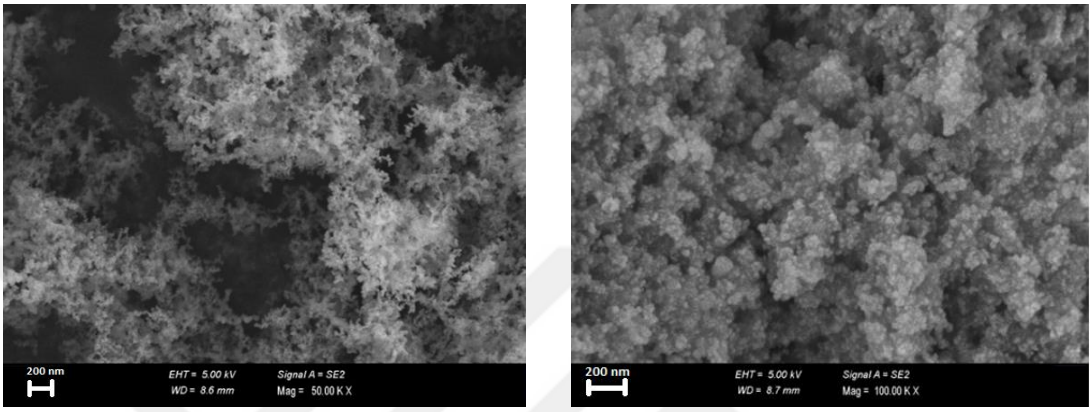


Figure 5.3 SEM images of SiO_2 nanoparticles with 50K and 100K magnitude

5.1.4 Organic Bond Structures

As a result of the FT-IR analysis (Fig. 5.4), peaks of 795 and 1046 cm^{-1} were observed in SiO_2 nanoparticle samples. They were expected to be observed since they are characteristic peaks showing O-Si-O and Si-O-Si bonds. The peak seen at 1635 cm^{-1} was observed due to the water in SiO_2 (Yang D. L., et al., 2020). When looking at the spectrum showing SiO_2 nanoparticles coated with silane material, a peak of 1718 cm^{-1} was observed, representing the C=O bonds in the methacrylate group contained in the MPS used as the coating material. The peak observed at 1458 cm^{-1} is attributed to the C-H stretching in the MPS structure (Rhee S. H. et al., 2002). These peaks observed as a result of FT-IR analysis and the bonds they represent prove that the silanization process has occurred.

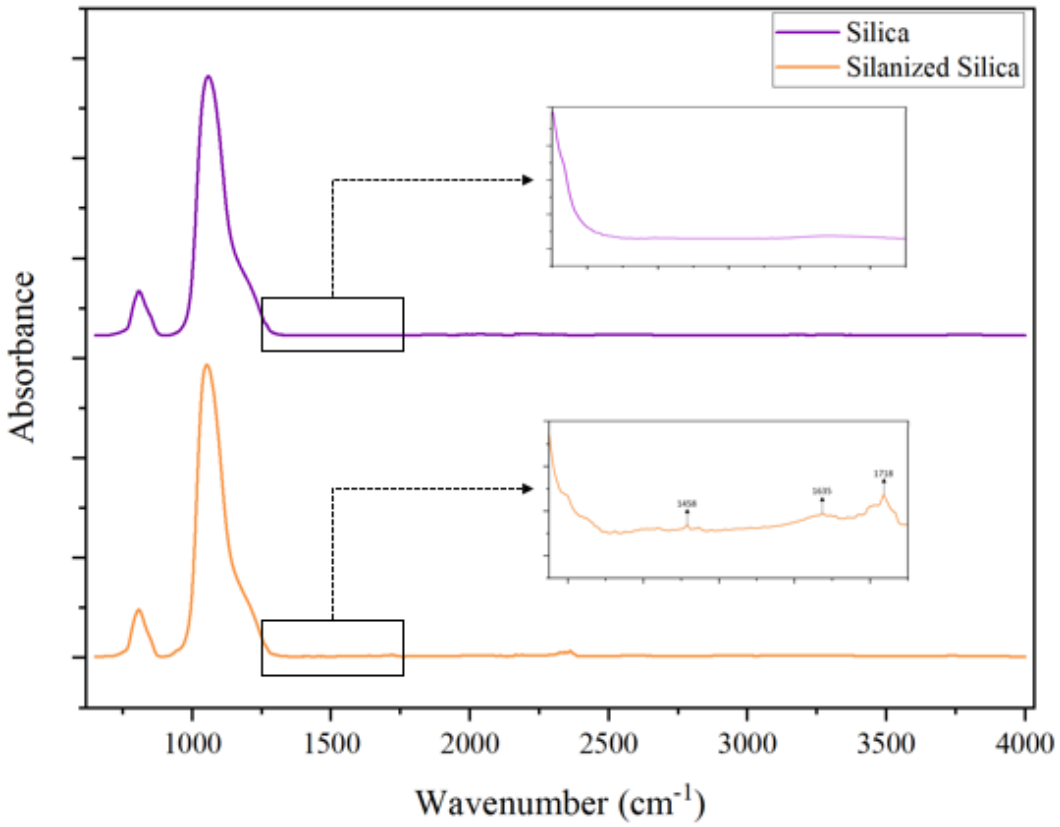


Figure 5.4 FT-IR Spectra of unsilanized and silanized SiO_2 nanoparticles

5.1.5 Particle Size

The particle size distribution graph of SiO_2 nanoparticles dispersed in IPA is presented in Figure 5.5. Upon careful examination of the graphs, it is evident that the particles are in the nano size range. Particle sizes appear to be distributed between approximately 60 and 1000 nm. It has been determined that these results are more accurate, especially since particles of 100 nm and below do not agglomerate. The average particle size was determined as 215 nm. Although the particle sizes are higher than expected due to agglomeration, SEM images of the nanoparticles show that they are approximately 100 nm.

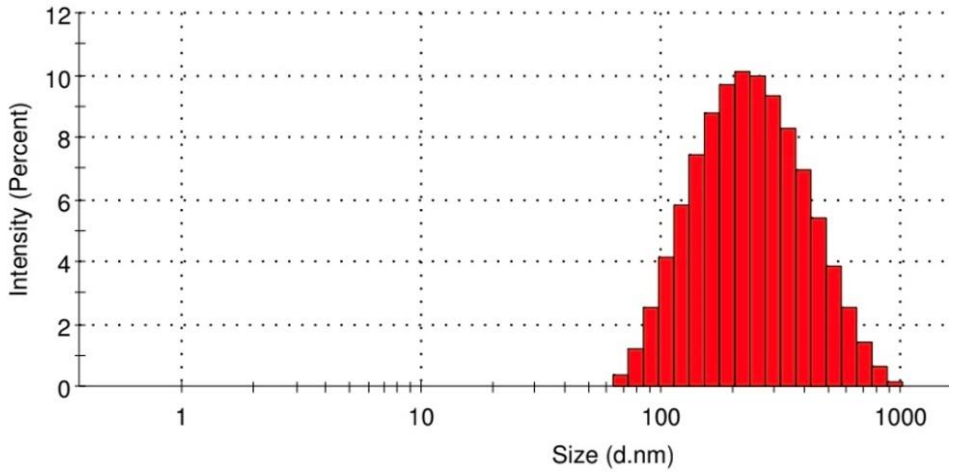


Figure 5.5 Particle Size Distribution of SiO_2 Nanoparticles

5.2 Characterization of Nanocomposite Resins

5.2.1 Morphological Properties

Palucci Rosa et al., saw in their study that, the mechanical properties of reinforced composites are commonly influenced by two critical factors: The uniform distribution of filler nanoparticles and the strength of interfacial interaction (Palucci Rosa et al., 2022). The attainment of a consistent dispersion of fillers and the development of robust interfacial bonds contribute to the remarkable performance of nanocomposites. Figure 5.6a illustrates pure ecoresin, while Figure 5.6b depicts the distribution of silanized nanoparticles in ecoresin, and Figure 5.6c displays unsilanized nanoparticles' distribution in ecoresin. Looking at Figure 5.6a, particle-like structures can be seen scattered across the cross-section. Since no nanoparticles were added to this sample, it was thought that what was seen in the structure might be palladium and gold from the coating. Protective additives can also be added to ready-made resins during their production, and these may be the observed structures. Looking at Figure 5.6b and Figure 5.6c, it is seen that nanoparticles are dispersed into the resin and larger particles are also observed in places. The reason for larger particles being seen is attributed to agglomeration.

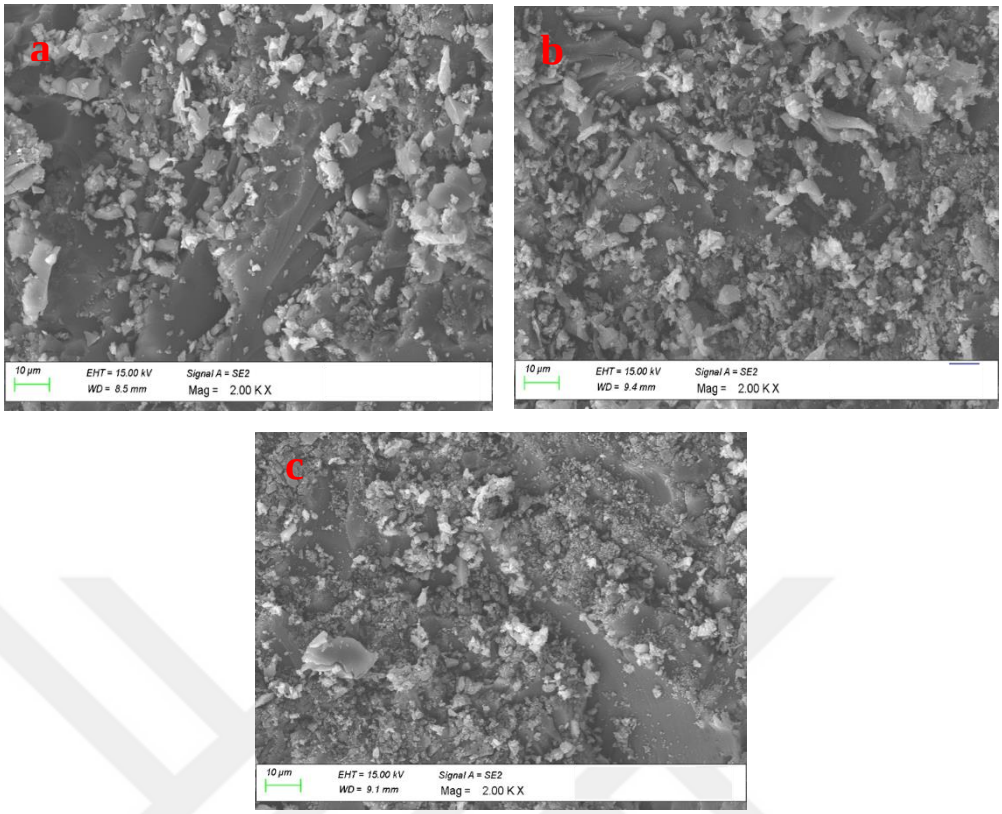


Figure 5.6 SEM images of ecoresin (a) EC1.5 (b) SEC1.5 (c)

In order to better understand the SEM images, EDS analysis was performed on the relevant samples. As a result of EDS, the components in the structure are shown for the EC sample, SEC1.5 sample and EC1.5 sample, respectively (Figure 5.7).

It was seen with the EDS analysis performed after the SEM analysis; C and O, which come from the organic structure of the resin, were detected in all three samples and their distributions are shown with EDS map images. (Fig 5.7). Looking at Fig. 5.7, it is thought that the presence of phosphorus was found in all three samples due to the phosphorus found in the structure of the photoinitiator (Diphenyl (2,4,6-trimethylbenzoyl) phosphine oxide-TPO) used within the scope of this thesis. The silicon seen in EC1.5 and SEC1.5 samples is supported by map images. When the images were examined, agglomeration was detected in the SEC1.5 sample, therefore it was determined that the silanization process did not have a negative effect on agglomeration.

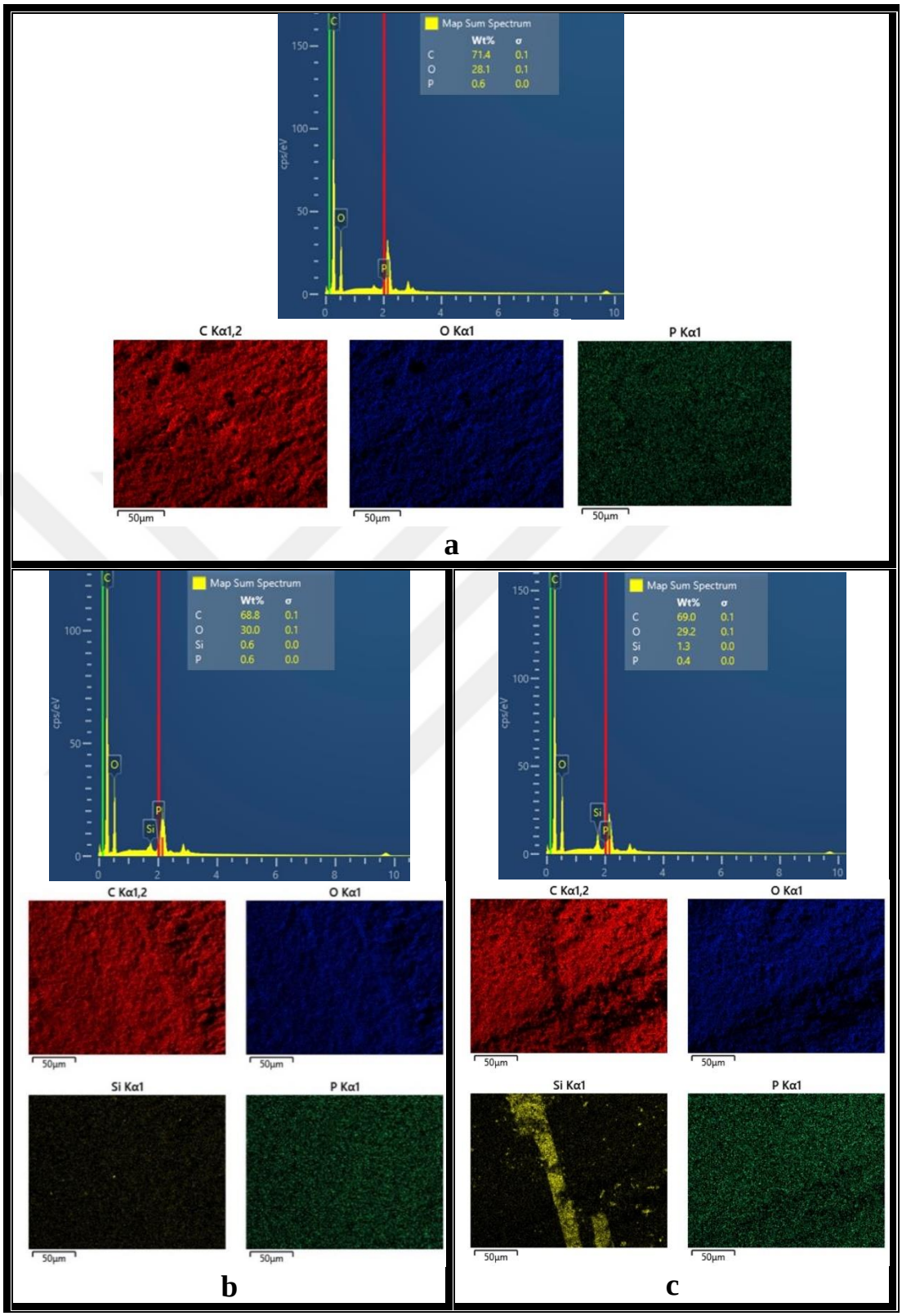


Figure 5.7 X-ray mapping and EDS results of ecoresin (a), EC1.5 (b) SEC1.5 (c)

5.2.2 Organic Bond Structures

Fourier Transform Infrared (FT-IR) spectroscopy was utilized to examine the organic bond configurations and transformation degrees of the commercial resin and composites. In order to determine the degree of transformation, FT-IR analysis was performed on the prepared samples before and after the printing process. In this way, C-C and C=C bonds existing in the structure were detected. Equation 5.1 was used to calculate transformation degrees.

$$DC = 1 - \left(\frac{A_{C=C(t)}}{A_{C=C(0)}}\right) \tag{5.1}$$

$A_{C=C(0)}$ seen in equation 5.1 represents the density of C=C bonds in the 1637 cm^{-1} peak before the polymerization process, and $A_{C=C(t)}$ represents the density after polymerization. The A_C sample is observed with FT-IR to evaluate before and after polymerization (Figure 5.8). The conversion degrees of all samples were calculated by taking the average of three measurements and are shown in Figure 5.9.

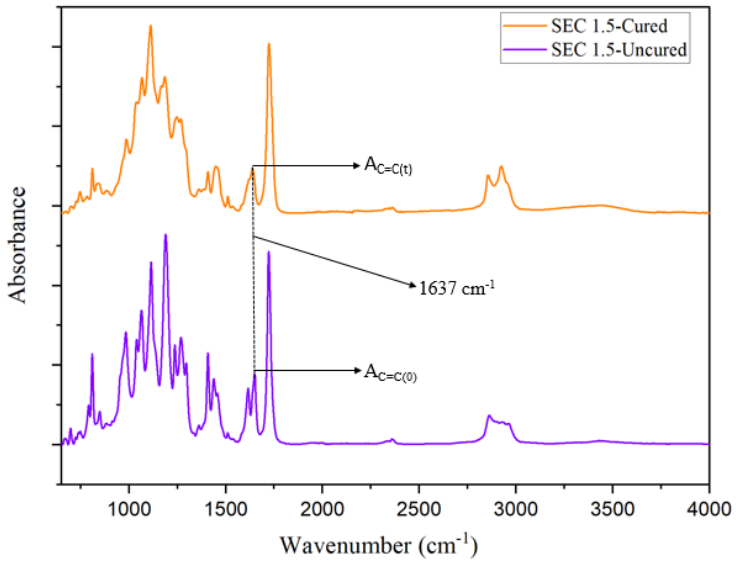


Figure 5. 8 FT-IR chart of SEC 1.5 sample before and after curing

As shown in Figure 5.9, the silanization procedure exhibited a positive effect on the conversion rate. This outcome is attributed to the interaction between the acrylate groups in the silane compound and those present in the resin during the curing process. As seen in the study of Yang D. L. et al., this interaction leads to an enhancement in bond conversion, resulting in an overall increase in the conversion level. In the case of

the reinforced materials, both SEC1.5 and SEC5 exhibited the most favorable results in terms of the conversion degree, demonstrating respective increases of 8.5% and 9.1%. Conversely, the lowest conversion degree observed in the EC2 sample is attributed to the potential agglomeration of powder within the structure, which could hinder the polymerization process (Yang D. L., et al., 2020).

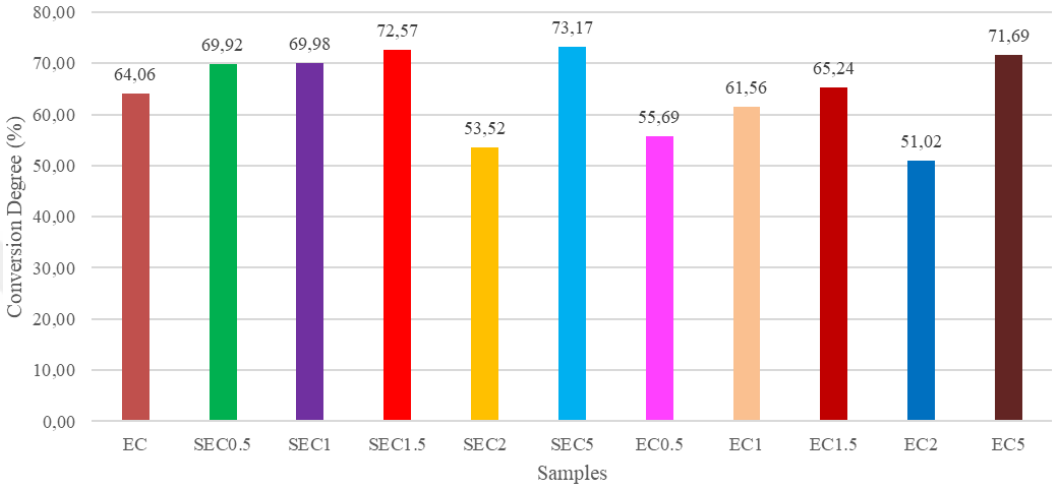


Figure 5.9 Conversion Degrees of Samples

5.2.3 Mechanical Properties

The mechanical properties of the prepared samples were obtained through three-point bending and tensile tests and the results are shown in Figure 5.10. With the addition of SiO_2 nanoparticles, positive effects were observed on elasticity modulus and flexural strength values. Previous studies have also shown that SiO_2 additive improves mechanical properties (Brusenteva et al., 2015). Furthermore, specimens containing SiO_2 coated with silane exhibit superior performance in mechanical tests, attributed to the silanization process. This process reduces the likelihood of particle agglomeration and alleviates stress concentration. The mean of elasticity modulus values was calculated as 2.73 and the standard deviation was 0.18. The mean of flexural strength values was calculated as 76.82 and the standard deviation was 13.4. The average of yield strength values was calculated as 29.6 and the standard deviation was 3.01.

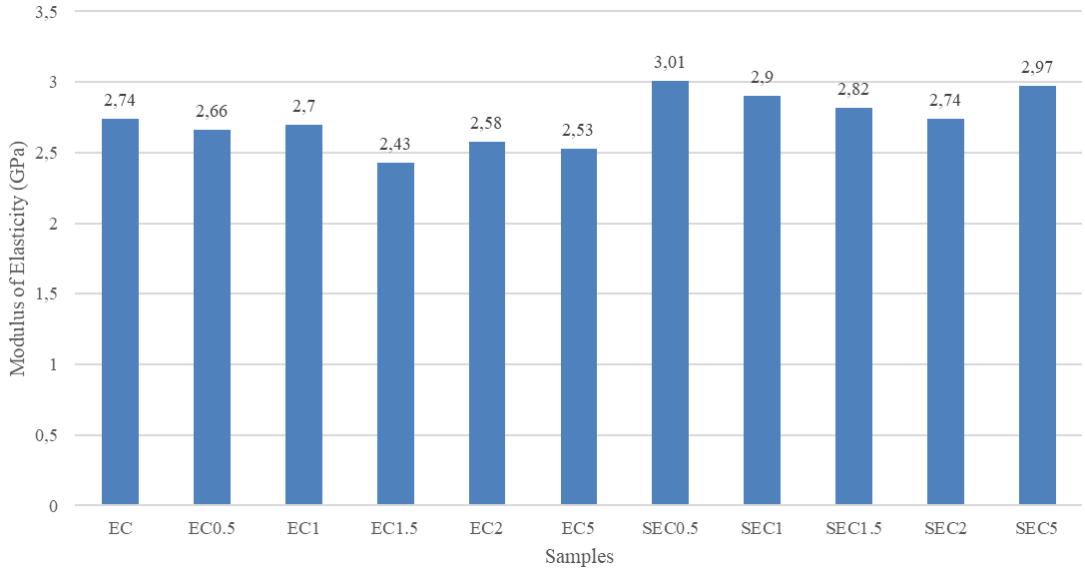


Figure 5.10 Elasticity Modulus Graph of Samples

According to the Balguri, P. K., et al, upon examining the elastic modulus values, it was noted that nanocomposites formulated with silanized nanoparticles exhibited superior outcomes compared to those prepared with non-silanated nanoparticles. (Balguri, P. K., et al.,2021). Elastic modulus values vary inversely with the brittleness of the material. It is normal for the elasticity modulus values to decrease, especially as a result of the addition of ceramic materials to the structure. However, since silanized nanoparticles increased adhesion to the polymer structure, an increase in the elasticity modulus results was observed. This suggests a reduction in the agglomeration of silanized nanoparticles within the resin, leading to a more homogeneous distribution of particles. Among all the samples, the SEC0.5 sample yielded the most favorable result. Elasticity modulus values are parallel to the transformation degree values, and positive results of the silanization process are observed in both.

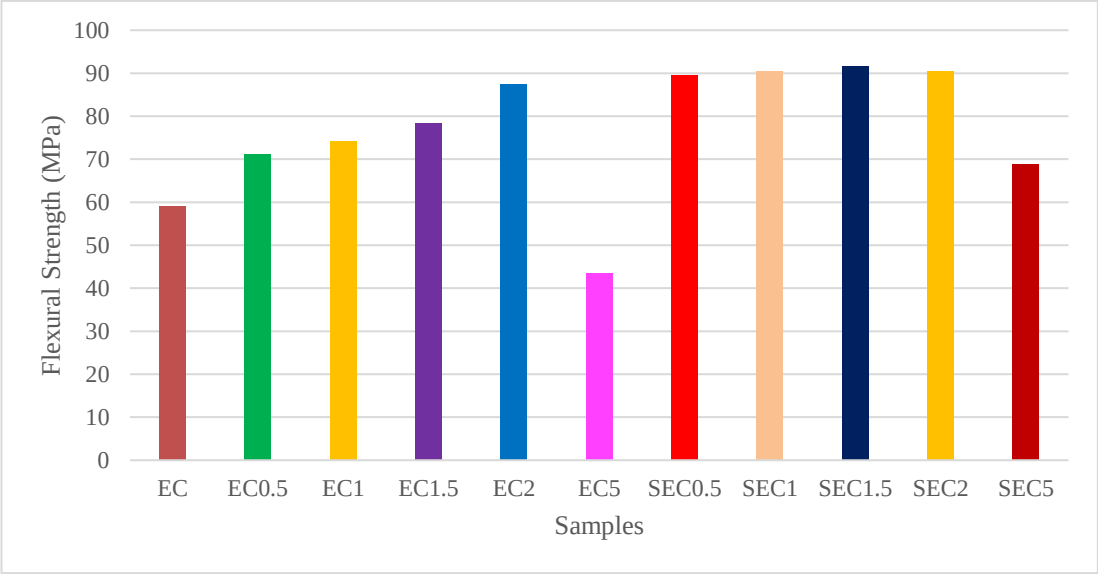


Figure 5.11 Flexural Strengths of Samples

Upon scrutinizing the flexural strength values presented in Figure 5.11, it is noteworthy to mention that, as documented in the literature, an escalation in the SiO_2 ratio tends to correlate with an improvement in flexural strength values (Rezvani M.B. et al., 2015). It was observed that the felxural strength value increased approximately 1.5 times, especially with the addition of silanized nanoparticles. Notably, the outcomes of the silanized samples exhibit an increase, attributed to the diminished agglomeration of nanoparticles within the resin. This reduced agglomeration results in a more uniform distribution of the silanized nanoparticles. Remarkably, it was observed that the most favorable result emanated from the SEC1.5 sample.

Figure 5.12 shows the yield strength results. It was observed that samples prepared with silanized nanoparticles exhibited higher values than samples prepared with non-silanized nanoparticles. The SEC5 sample gave the best result, which shows that increasing the additive rate positively affected the yield strength value.

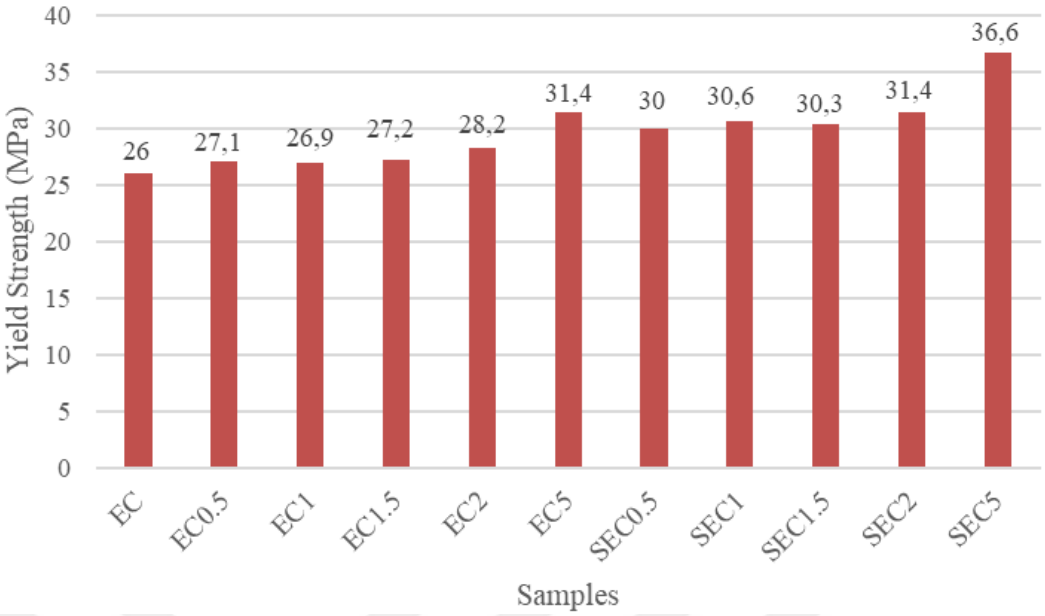


Figure 5.12 Yield Strengths of Samples

5.2.4. Hardness Tests

Hardness measurements of samples were made five times on each sample and the averages of the obtained values are shown in Figure 5.13. It is known that polymers give values between 30 and 95 as a result of the Shore D test, in this sense the results are consistent (Alshabib, A. et al., 2019). As a result of the analysis, no significant differences were observed between the surface hardness values of the samples.

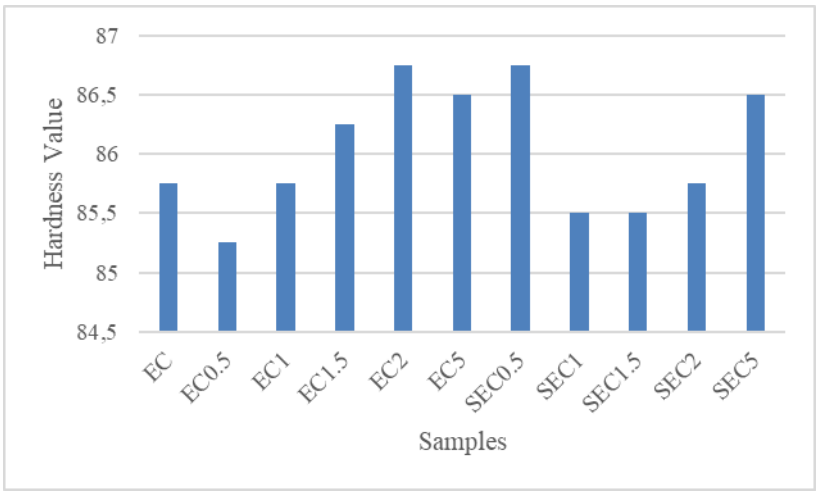


Figure 5.13 Hardness Values of Samples

5.2.5 XPS Analysis

As a result of the XPS analysis (Fig. 5.14, 5.15 and 5.16) performed with SEC1.5, EC1.5 and EC samples, the elemental contents of the samples were examined. The fact that the silica peak is at or around 103 eV indicates that silica is in oxide form (Stakheev, A. Et al., 1993). The phosphorus found in the samples as a result of the analysis is thought to originate from TPO (Trimethylbenzoyl diphenylphosphine oxide), which is widely used as a photoinitiator. While EC has the highest carbon content among the samples, SEC1.5 has the lowest content as can be seen in Table 5.1.

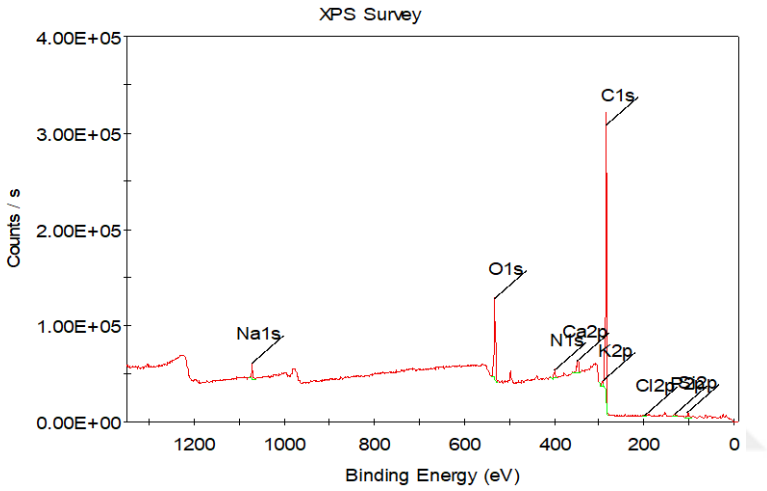


Figure 5.14 XPS spectra of SEC1.5

Table 5.1 XPS Analysis Contents of SEC1.5

Name	***Peak BE eV***	***Weight %***
K2p	293.14	0.76
C1s	284.29	71.61
O1s	531.96	14.75
Na1s	1071.84	1.61
N1s	399.10	2.32
Ca2p	347.07	3.03
Si2p	102.89	5.60
Cl2p	198.73	0.76
P2p	131.86	1.56

Elements such as K, Ca, Cl and Na are pollution sources, and as can be seen in Table 5.1, Table 5.2 and Table 5.3, C, O and P elements were found in all three samples. C and O come from organic structure. It is thought that the presence of trace amounts of silica in the pure EC sample is due to pollution in the printer chamber.

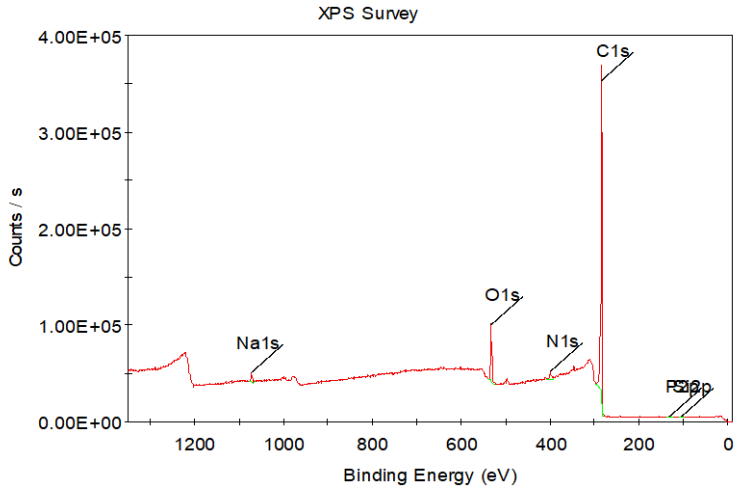


Figure 5.15 XPS spectra of EC1.5

Table 5.2 XPS Analysis Contents of EC1.5

Name	***Peak BE eV***	***Weight %***
C1s	284.36	75.35
O1s	532.67	13.03
Si2p	103.10	6.17
N1s	399.17	1.95
Ca2p	347.22	1.07
Na1s	1072.13	0.52
P2p	131.26	1.91

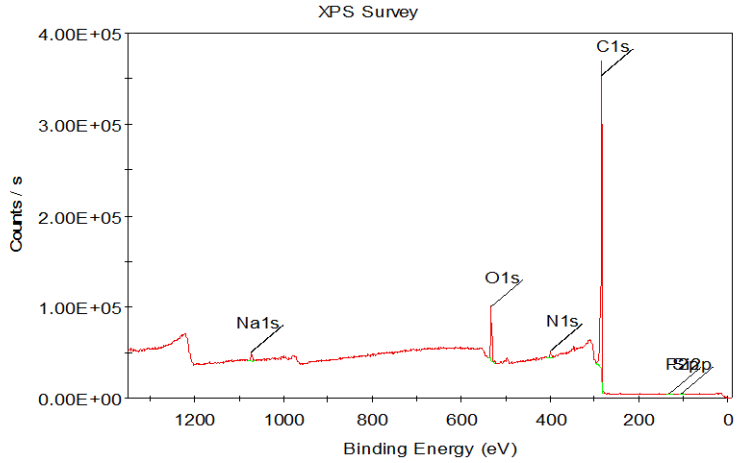


Figure 5.16 XPS spectra of EC

As the amount of nanoparticles added to the sample increases, a decrease is observed in the amount of carbon, which is the organic component SEC1.5 and EC1.5. Even though no significant difference is observed between the carbon contents of

SEC1.5 and EC1.5 samples, the existing difference is thought to be due to the silane material (Table 5.1 and Table 5.2).

Table 5.3 XPS Analysis Contents of EC

Name	***Peak BE eV***	***Weight %***
C1s	284.28	84.83
O1s	532.19	10.14
N1s	399.10	2.31
Na1s	1071.90	1.19
Si2p	102.78	0.93
P2p	131.43	0.60

5.2.6 Structural Properties

XRD spectra of nanocomposite samples are seen in Figure 5.17. When looking at the spectra, it is seen that the samples are polymers. When looking at the spectra, it can be seen that the structures are amorphous.

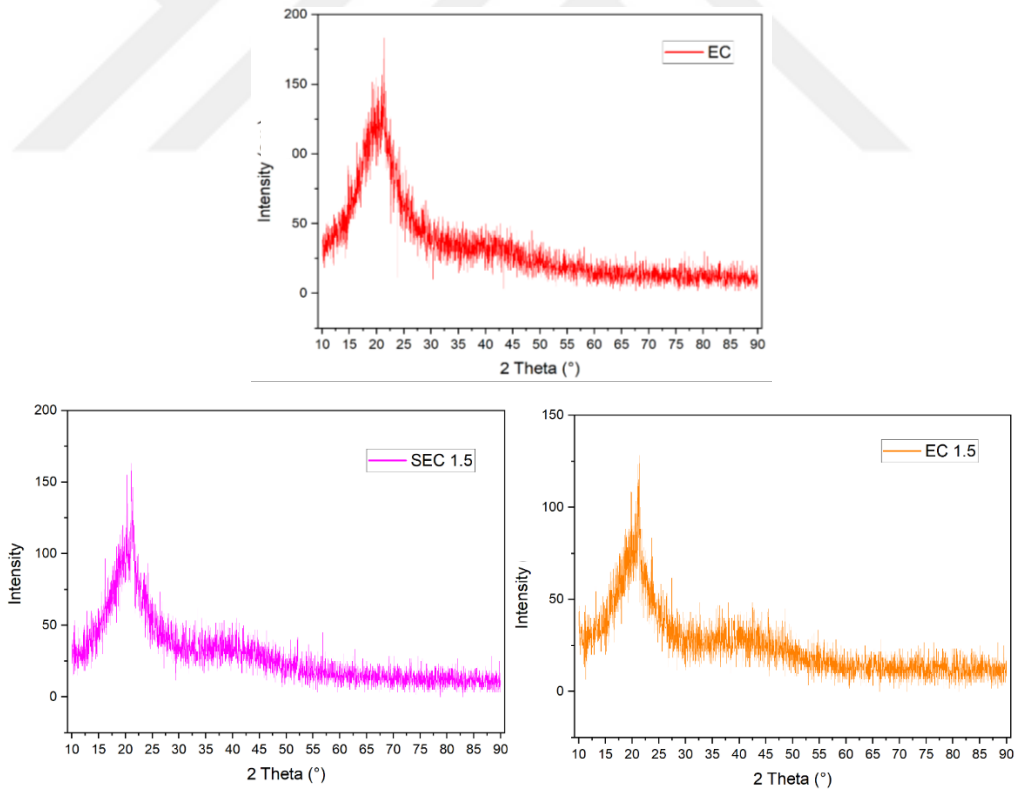


Figure 5.17 XRD paterns of nanocomposites

Figure 5.17 presents the X-ray diffraction (XRD) evaluation plot, which reveals a broad peak characteristic of amorphous silica. The diffraction angle (2θ) ranges from 10° to 30°. However, the introduction of silica nanoparticles into the pure resin induces a significant increase in intensity. This observation aligns with published research, suggesting the formation of cross-linked and/or integrated polymer chains within the SiO_2 phase through covalent and hydrogen bonds (Tomić, M. Et al., 2019).

5.2.7 Thermal Properties

Thermogravimetric and differential thermal analysis (PerkinElmer, STA8000) were performed to determine the heat treatment parameters. The test was carried out in a nitrogen atmosphere, the temperature range was set as 0 – 1000 °C and the increase rate was determined as 5 °C/min.

When the loss rates are compared, it is seen that the sample containing silane nanoparticles loses slightly more with temperature due to its higher organic content.

In Figure 5.18., when T onset and T end temperatures were examined, it was decided that the additives to the resin did not cause a significant change in thermal properties, since no significant difference was seen. No significant difference was observed between the weight loss values of EC, EC1.5 and SEC1.5 samples. The weight loss values of the samples are 92.6, 91.7 and 92 percent, respectively.

The stage of heat degradation of the soybean oil backbone occurred between 290 and 540 °C. Hong J. et al. have previously documented similar two-stage breakdown behaviors from thermosets based on soybean oil. Furthermore, at about 800 °C, the breakdown process resulted in the creation of a little char (13%), which almost completely reduced the weight (87%) (Hong J., et al., 2012).

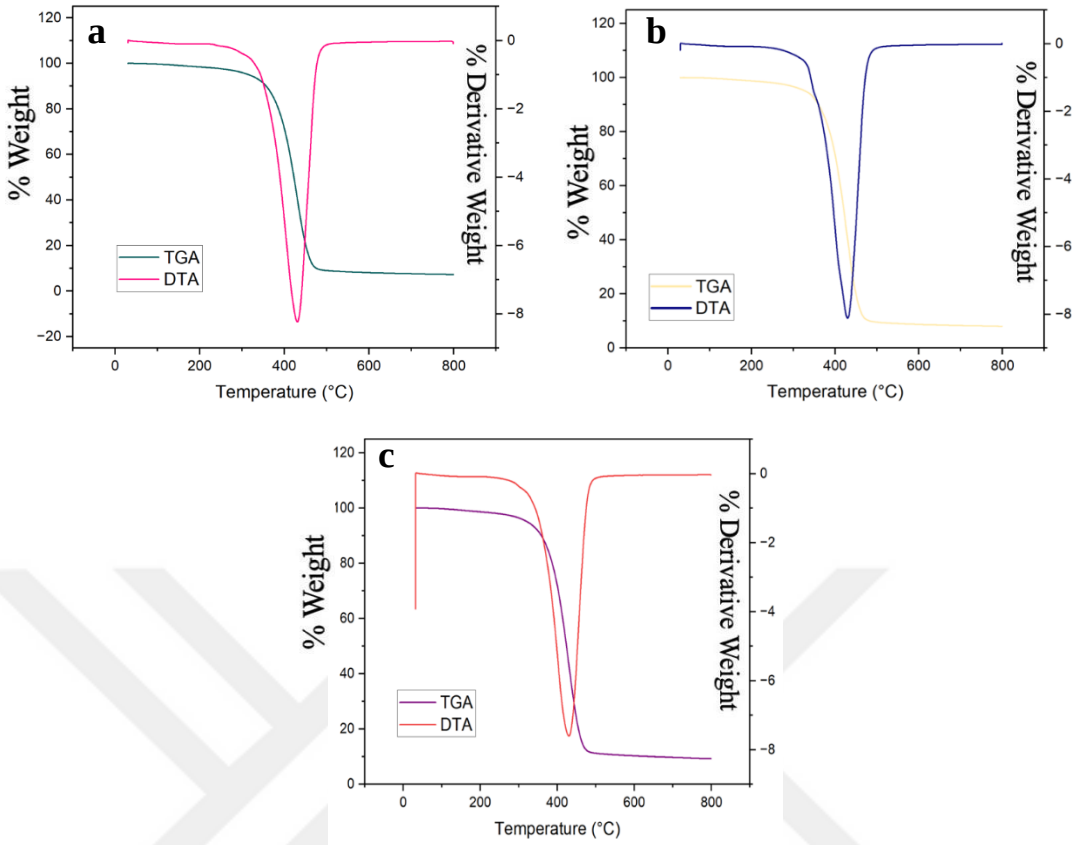


Figure 5.18 DTA-TGA graph of EC (a), SEC1,5 (b) and EC1,5 (c)

5.2.8 Viscosity

The viscosity properties of pure ecoresin and liquid nanocomposites prepared in different compositions were determined with a rheometer device. According to Mondschein, R. J. et al, resins used in SLA-DLP type printers can have viscosities as high as 1 Pa.s; however, this value varies from 0.25 Pa.s for low molecular weight and/or diluted materials to 10 Pa.s for samples with greater molecular weights. As a result of the analysis, all samples were found to be suitable for printing and the results are given in Figure 5.19 and Table 5.4 (Mondschein, R. J. et al., 2017).

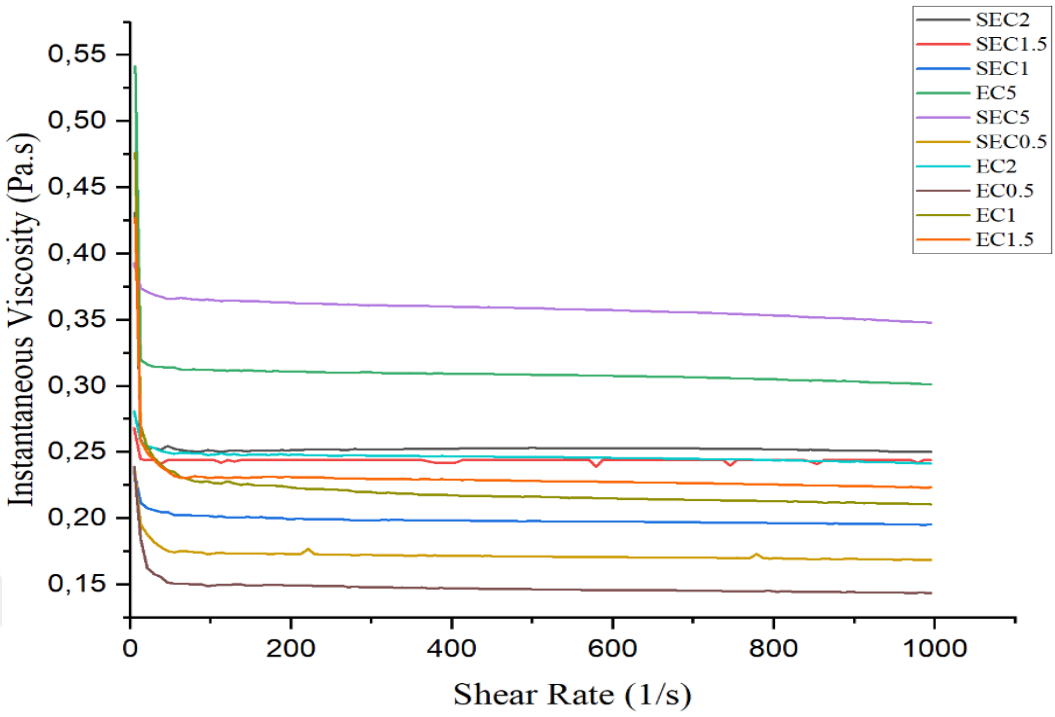


Figure 5.19 Rheometer measurement of nanocomposites

Table 5.4 Viscosity Values

Sample Name	***Viscosity Value (Pa.s)***
SEC0.5	0.17
SEC1	0.2
SEC1.5	0.24
SEC2	0.26
SEC5	0.36
EC0.5	0.15
EC1	0.22
EC1.5	0.23
EC2	0.25
EC5	0.32

CHAPTER SIX
CONCLUSION AND FUTURE WORKS

The successful execution of the production and subsequent printing of nanocomposite resins, enhanced with SiO_2, is the focus of this section. It aims to provide a thorough overview of the characterizations performed throughout the entire production process. The sol-gel method emerged as the chosen technique for both nanoparticle production and silanization processes, ultimately yielding SiO_2 nanoparticles with an amorphous quartz-phase structure. The formulation of composite samples ensued by blending these synthesized powders with the existing resin in carefully calibrated proportions.

The focus of the examination centered predominantly on assessing the transformation degrees and mechanical properties exhibited by the resulting samples. Notably, special attention was given to the SEC1.5 sample, wherein detailed documentation of particle ratios was conducted. This specific sample showcased particularly favorable outcomes across various analyses, underscoring its significance in the context of the study. The detailed investigation of these key aspects contributes to a comprehensive understanding of the successful synthesis and performance evaluation of SiO_2-reinforced nanocomposite resins in the course of this research endeavor.

In future studies on this subject, different materials can be used to silanize SiO_2 nanoparticles and the effects of this can be examined. Instead of biobased resin obtained from soybean oil, studies can be carried out with biobased resins obtained from other raw materials. Different results can be obtained by changing the parameters of three-dimensional printing.

REFERENCES

Åkesson, D., Skrifvars, M., Lv, S., Shi, W., Adekunle, K., Seppälä, J., & Turunen, M. (2010). Preparation of nanocomposites from biobased thermoset resins by UV-curing. Progress in Organic Coatings, 67(3), 281-286.

Alshabib, A., Silikas, N., & Watts, D. C. (2019). Hardness and fracture toughness of resin-composite materials with and without fibers. Dental Materials, 35(8), 1194-1203.

Altuna, F. I., Espósito, L. H., Ruseckaite, R. A., & Stefani, P. M. (2011). Thermal and mechanical properties of anhydride-cured epoxy resins with different contents of biobased epoxidized soybean oil. Journal of Applied Polymer Science, 120(2), 789-798.

Bagheri, A., & Jin, J. (2019). Photopolymerization in 3D printing. ACS Applied Polymer Materials, 1(4), 593-611.

Balguri, P. K., Samuel, D. H., & Thumu, U. (2021). A review on mechanical properties of epoxy nanocomposites. Materials Today: Proceedings, 44, 346-355.

Bao, Y., Paunović, N., & Leroux, J.-C. (2022). Challenges and Opportunities in 3D Printing of Biodegradable Medical Devices by Emerging Photopolymerization Techniques. Advanced Functional Materials, 32(15), 2109864.

Barszczewska-Rybarek, I. M. (2012). Quantitative determination of degree of conversion in photocured poly (urethane-dimethacrylate) s by Fourier transform infrared spectroscopy. Journal of applied polymer science, 123(3), 1604-1611.

Bokov, D., Turki Jalil, A., Chupradit, S., Suksatan, W., Javed Ansari, M., Shewael, I. H., ... & Kianfar, E. (2021). Nanomaterial by sol-gel method: synthesis and application. Advances in Materials Science and Engineering, 2021, 1-21.

Bonnaillie, L. M. (2004). Method for the Fabrication of Bio0based Thermoset Foam from Acrylated Epoxidized Soybean Oil (Doctoral dissertation, University of Delaware)

Brusentseva, T. A., Filippov, A. A., Fomin, V. M., Smirnov, S. V., & Veretennikova, I. A. (2015). Modification of epoxy resin with silica nanoparticles and process engineering of composites based on them. Mechanics of Composite Materials, 51, 531-538.

Cho, J. D., Kim, Y. B., Ju, H. T., & Hong, J. W. (2005). The effects of silica nanoparticles on the photocuring behaviors of UV-curable polyester acrylate-based coating systems. Macromolecular Research, 13, 362-365.

Chung, K. H., & Greener, E. H. (1990). Correlation between degree of conversion, filler concentration and mechanical properties of posterior composite resins. Journal of oral rehabilitation, 17(5), 487-494.

Gorji, B., Ghasri, M. A., Fazaeli, R., & Niksirat, N. (2012). Synthesis and characterizations of silica nanoparticles by a new sol-gel method. Journal of Applied Chemical Research, 6(3), 22-26.

Gryglewicz, S., Piechocki, W., & Gryglewicz, G. (2003). Preparation of polyol esters based on vegetable and animal fats. Bioresource Technology, 87(1), 35-39.

Guit, J., Tavares, M. B., Hul, J., Ye, C., Loos, K., Jager, J., ... & Voet, V. S. (2020). Photopolymer resins with biobased methacrylates based on soybean oil for stereolithography. ACS Applied Polymer Materials, 2(2), 949-957.

Guleria, A. N., & Salhotra, S. (2016). Effects of silica fume (micro silica or nano silica) on mechanical properties of concrete: A review. Int. J. Civ. Eng. Technol, 7(4), 345-357.

Guleria, A. N., & Salhotra, S. (2016). Effects of silica fume (micro silica or nano silica) on mechanical properties of concrete: A review. Int. J. Civ. Eng. Technol, 7(4), 345-357.

Gülcan, O., Günaydın, K., & Tamer, A. (2021). The state of the art of material jetting—a critical review. Polymers, 13(16), 2829.

Gürmen, S., Ebin, B., & İtü, M. (2008). Nanopartiküller ve üretim yöntemleri-1. Metalurji Dergisi, 150, 31-38.

Herbeck, L., Mahrholz, T., Mosch, J., Riedel, U., & Rostermundt, D. (2005). Faser verstarkte Nanocomposites--Stand der Technik und Perspektiven. Gummi Fasern Kunststoffe, 58(3), 161-165.

Ho, C. M. B., Ng, S. H., & Yoon, Y. J. (2015). A review on 3D printed bioimplants. International Journal of Precision Engineering and Manufacturing, 16, 1035-1046.

Hong J, Luo Q, Wan X, Petrovi´c ZS and Shah BK, Biomacromolecules13:261–266 (2012).

Jacobs, P. F. (1992). Fundamentals of stereolithography. 1992 International Solid Freeform Fabrication Symposium.

Jafarzadeh, M., Rahman, I. A., & Sipaut, C. S. (2009). Synthesis of silica nanoparticles by modified sol–gel process: the effect of mixing modes of the reactants and drying techniques. Journal of Sol-Gel Science and Technology, 50, 328-336.

Jagtap, A. R., & More, A. (2022). Developments in reactive diluents: a review. Polymer Bulletin, 79(8), 5667-5708.

Kabir, S. F., Mathur, K., & Seyam, A. F. M. (2020). A critical review on 3D printed continuous fiber-reinforced composites: History, mechanism, materials and properties. Composite Structures, 232, 111476.

Kavaz, D. (2022). Synthesis of silica nanoparticles from agricultural waste. In Agri-Waste and Microbes for Production of Sustainable Nanomaterials (pp. 121-138). Elsevier.

Kowalska, A., Sokolowski, J., & Bociong, K. (2021). The Photoinitiators Used in Resin Based Dental Composite—A Review and Future Perspectives. Polymers 2021, 13, 470.

Li, X., Lin, H., Jiang, H., Zhang, Y., Liu, B., Sun, Y., & Zhao, C. (2021). Preparation and properties of a new bio-based epoxy resin/diatomite composite. Polymer Degradation and Stability, 187, 109541.

Liu, C., Qian, B., Liu, X., Tong, L., & Qiu, J. (2018). Additive manufacturing of silica glass using laser stereolithography with a top-down approach and fast debinding. RSC advances, 8(29), 16344-16348.

Liveri, V. T., 2006. Controlled Synthesis of Nanoparticles in Microheterogeneous Systems, Springer Science+Business Media, Inc., New York.

Lung, C. Y., & Matinlinna, J. P. (2010). Resin bonding to silicatized zirconia with two isocyanatosilanes and a cross-linking silane. Part I: experimental. Silicon, 2, 153-161.

Lung, Y. K., & Matinlinna, J. P. (2013). Silanes for adhesion promotion and surface modification. Silane: chemistry, applications and performance.

Maines, E. M., Porwal, M. K., Ellison, C. J., & Reineke, T. M. (2021). Sustainable advances in SLA/DLP 3D printing materials and processes. Green Chemistry, 23(18), 6863-6897.

Mazzoli, A. (2013). Selective laser sintering in biomedical engineering. Medical & biological engineering & computing, 51, 245-256

Mohamed, O. A., Masood, S. H., & Bhowmik, J. L. (2015). Optimization of fused deposition modeling process parameters: a review of current research and future prospects. Advances in Manufacturing, 3(1), 42–53.

Mondschein, R. J., Kanitkar, A., Williams, C. B., Verbridge, S. S., & Long, T. E. (2017). Polymer structure-property requirements for stereolithographic 3D printing of soft tissue engineering scaffolds. Biomaterials, 140, 170-188.

Mostafaei, A., Elliott, A. M., Barnes, J. E., Li, F., Tan, W., Cramer, C. L., ... & Chmielus, M. (2021). Binder jet 3D printing—Process parameters, materials, properties, modeling, and challenges. Progress in Materials Science, 119, 100707.

Munir, K. S., Li, Y., & Wen, C. (2017). Metallic scaffolds manufactured by selective laser melting for biomedical applications. In Metallic Foam Bone (pp. 1-23). Woodhead Publishing.

Mustapha, R., Rahmat, A. R., Abdul Majid, R., & Mustapha, S. N. H. (2019). Vegetable oil-based epoxy resins and their composites with bio-based hardener: A short review. Polymer-Plastics Technology and Materials, 58(12), 1311-1326.

Nandy, J., Sarangi, H., & Sahoo, S. (2019). A review on direct metal laser sintering: Process features and microstructure modeling. Lasers in Manufacturing and Materials Processing, 6(3), 280-316.

Ou, C. F., & Shiu, M. C. (2010). Epoxy composites reinforced by different size silica nanoparticles. Journal of applied polymer science, 115(5), 2648-2653.

Palucci Rosa, R., & Rosace, G. (2021). Nanomaterials for 3D printing of polymers via stereolithography: Concept, technologies, and applications. Macromolecular Materials and Engineering, 306(10), 2100345.

Palucci Rosa, R., Rosace, G., Arrigo, R., & Malucelli, G. (2022). Preparation and Characterization of 3D-Printed Biobased Composites Containing Micro-or Nanocrystalline Cellulose. Polymers, 14(9), 1886.

Penumakala, P. K., Santo, J., & Thomas, A. (2020). A critical review on the fused deposition modeling ofthermoplastic polymer composites. Composites Part B: Engineering, 201, 108336.)

Quirino, R. L., Woodford, J., & Larock, R. C. (2012). Soybean and linseed oil-based composites reinforced with wood flour and wood fibers. Journal of applied polymer science, 124(2), 1520-1528.

Rhee, S. H., & Choi, J. Y. (2002). Preparation of a bioactive poly (methyl methacrylate)/silica nanocomposite. Journal of the American Ceramic Society, 85(5), 1318-1320.

Rezvani, M. B., Atai, M., Hamze, F., & Hajrezai, R. (2016). The effect of silica nanoparticles on the mechanical properties of fiber-reinforced composite resins. Journal of Dental Research, Dental Clinics, Dental Prospects, 10(2), 112.

Rosso, P., Ye, L., Friedrich, K., & Sprenger, S. (2006). A toughened epoxy resin by silica nanoparticle reinforcement. Journal of Applied Polymer Science, 100(3), 1849-185

Salonitis K. 2014.Stereolithography. Compr. Mater. Process., vol. 10, Elsevier Ltd; , p. 19–67.

Sarac, M., Oranlı, A., Aktitiz, İ., Yalcin, B. S., & Varol, R. (2019). 3B Basılabilir Füme Silika Takviyeli Foto-Duyarlı Polimerlerin Mekanik Özelliklerinin İncelenmesi. Düzce Üniversitesi Bilim ve Teknoloji Dergisi, 7(3), 1793-1805.

Shajii, L., & Santerre, J. P. (1999). Effect of filler content on the profile of released biodegradation products in micro-filled bis-GMA/TEGDMA dental composite resins. Biomaterials, 20(20), 1897-1908.

Shibata, M. (2011). Bio-based nanocomposites composed of photo-cured soybean-based resins and supramolecular hydroxystearic acid nanofibers. Mol. Aspects Breed, 12, 473-494.

Shnoudeh, A. J., Hamad, I., Abdo, R. W., Qadumii, L., Jaber, A. Y., Surchi, H. S., & Alkelany, S. Z. (2019). Synthesis, characterization, and applications of metal nanoparticles. In Biomaterials and bionanotechnology (pp. 527-612).

Silva, A. L., Salvador, G. M. D. S., Castro, S. V., Carvalho, N. M., & Munoz, R. A. (2021). A 3D printer guide for the development and application of electrochemical cells and devices. Frontiers in Chemistry, 9, 439.

Singh, L. P., Bhattacharyya, S. K., Kumar, R., Mishra, G., Sharma, U., Singh, G., & Ahalawat, S. (2014). Sol-Gel processing of silica nanoparticles and their applications. Advances in colloid and interface science, 214, 17-37.

Sprenger, S. (2013). Epoxy resins modified with elastomers and surface-modified silica nanoparticles. Polymer, 54(18), 4790-4797.

Sprenger, S. (2020). Nanosilica-toughened epoxy resins. Polymers, 12(8), 1777.

Sürmen, H. K. (2019). Eklemeli İmalat (3b Baskı): Teknolojiler Ve Uygulamalar. Uludağ Üniversitesi Mühendislik Fakültesi Dergisi, 24(2), 373-392.

Stakheev, A. Y., Shpiro, E. S., & Apijok, J. (1993). XPS and XAES study of titania-silica mixed oxide system. The Journal of Physical Chemistry, 97(21), 5668-5672.

Thielemans, W., Can, E., Morye, S. S., & Wool, R. P. (2002). Novel applications of lignin in composite materials. Journal of Applied Polymer Science, 83(2), 323-331.

Tomić, M., Dunjić, B., Nikolić, M. S., Stanković, N., Pavlović, V. B., Bajat, J., & Djonlagić, J. (2019). Polyamidoamine as a clay modifier and curing agent in preparation of epoxy nanocomposites. Progress in Organic Coatings, 131, 311-321.

Verma, A., Tyagi, S., & Yang, K. (2015). Modeling and optimization of direct metal laser sintering process. The International Journal of Advanced Manufacturing Technology, 77, 847-860.

Voet, V. S., Guit, J., & Loos, K. (2021). Sustainable photopolymers in 3d printing: A review on biobased, biodegradable, and recyclable alternatives. Macromolecular Rapid Communications, 42(3), 2000475.

Wang, L., Jiang, X., Wang, C., Huang, Y., Meng, Y., & Shao, J. (2020). Titanium dioxide grafted with silane coupling agents and its use in blue light curing ink. Coloration Technology, 136(1), 15-22.

Xu, X., Awad, A., Robles-Martinez, P., Gaisford, S., Goyanes, A., & Basit, A. W. (2021). Vat photopolymerization 3D printing for advanced drug delivery and medical device applications. Journal of Controlled Release, 329, 743-757.

Xu, X., Awad, A., Robles-Martinez, P., Gaisford, S., Goyanes, A., & Basit, A. W. (2021). Vat photopolymerization 3D printing for advanced drug delivery and medical device applications. Journal of Controlled Release, 329, 743-757.

Y. Rong, H. Z. Chen, G. Wu, and M. Wang, “Preparation and characterization of titanium dioxide nanoparticle/ polystyrene composites via radical polymerization,” Mater Chem Phys, vol. 91, no. 2–3, pp. 370–374, Jun. 2005, doi: 10.1016/j.matchemphys.2004.11.042.

Yang, D. L., Sun, Q., Niu, H., Wang, R. L., Wang, D., & Wang, J. X. (2020). The properties of dental resin composites reinforced with silica colloidal nanoparticle clusters: Effects of heat treatment and filler composition. Composites Part B: Engineering, 186, 107791.

Yang, H., Lim, J. C., Liu, Y., Qi, X., Yap, Y. L., Dikshit, V., ... & Wei, J. (2017). Performance evaluation of projet multi-material jetting 3D printer. Virtual and physical prototyping, 12(1), 95-103.

Yang, Z., Peng, S., Wang, Z., Miao, J. T., Zheng, L., Wu, L., & Weng, Z. (2022). UV-curable, low-viscosity resin with a high silica filler content for preparing ultrastiff, 3D-printed molds. ACS Applied Polymer Materials, 4(4), 2636-2647.

Zhang, C., Cui, Y., Li, J., & Jiang, D. (2015). Nano-sio2-reinforced ultraviolet-curing materials for three-dimensional printing. Journal of Applied Polymer Science, 132(31)

Zhang, J., & Xiao, P. (2018). 3D printing of photopolymers. Polymer Chemistry, 9(13), 1530-1540.

Ziaee, M., & Crane, N. B. (2019). Binder jetting: A review of process, materials, and methods. Additive Manufacturing, 28, 781-801.